PARAMETRIC EXCITATION OF A DWSC

A Thesis

by

CHANDAN LAKHOTIA

Submitted to the Office of Graduate Studies of
Texas A&M University
in partial fulfillment of the requirements for the degree of

MASTER OF SCIENCE

May 2010

Major Subject: Ocean Engineering

Parametric Excitation of a DWSC

PARAMETRIC EXCITATION OF A DWSC

A Thesis

by

CHANDAN LAKHOTIA

Submitted to the Office of Graduate Studies of
Texas A&M University
in partial fulfillment of the requirements for the degree of

MASTER OF SCIENCE

Approved by:

Chair of Committee,	Jeffrey M. Falzarano
Committee Members,	David A. Brooks
	Richard S. Mercier
Head of Department,	John M. Niedzwecki

May 2010

Major Subject: Ocean Engineering

ABSTRACT

Parametric Excitation of a DWSC. (May 2010)

Chandan Lakhotia, B.Tech., National Institute of Technology, Calicut

Chair of Advisory Committee: Dr. Jeffrey M. Falzarano

Parametric excitation of the DWSC (Deep Water Stable Craneship) is studied in this thesis. It occurs for a system without any external forcing, when one of the coefficients in the equation of motion (EOM) modeling the system varies with time. Parametric instability might be triggered for certain values of the parameters describing the time-varying coefficient. The DWSC, basically a stepped classic spar with a catamaran as its deck, because of certain unique features, may be susceptible to parametric excitation. This thesis examines the phenomenon of parametric excitation with respect to roll motion in head seas, using time-domain simulation and stability analysis. It examines the DWSC's susceptibility to parametric instability using the same methods of analysis and the effect of damping (especially viscous drag) on parametric excitation and instability. The thesis uses Mathieu's equation as the basis for stability analysis and time-simulates the coupled heave-sway-roll EOM.

Time-domain simulation is done for two reasons: firstly for determining the variation in roll stiffness because of a regular wave (the variation in roll stiffness is an input to the stability analysis) and secondly for simulating the coupled heave-sway-roll

EOM. Both time-domain analysis and stability analysis are done for sea states of interest and for examining interesting phenomena like roll resonance (due to body-wave interaction) and parametric instability.

Results highlight: 1) a ‘cancellation frequency’ in the heave wave exciting force; 2) the effect of viscous drag on coupled heave-sway-roll motions; 3) time-simulations validating the stability analysis; 4) the trend of stability with increasing sea states, wave periods and amplitudes; 5) characteristics of parametric instability; 6) the methodology used to predict or detect parametric instability and 7) the effect of viscous drag on parametric instability.

DEDICATION

To my mom and dad

ACKNOWLEDGEMENTS

First of all, I would like to thank Dr. Jeffrey Falzarano, my committee chair, for his invaluable support and guidance. This thesis and the research contained herein would not be possible without his encouragement. Secondly, I would like to thank Dr. David Brooks and Dr. Richard Mercier for being on my committee. Their dedication, both inside and outside the classroom, is truly inspirational. I would also like to thank the project sponsor, the Office of Naval Research, and program manager Kelly Cooper for letting me work on this project.

Finally, I would like to thank all my ‘friends’: everything made more sense ‘with a little help from my friends’.

TABLE OF CONTENTS

Page

LIST OF FIGURES

FIGURE Page

FIGURE Page

FIGURE Page

LIST OF TABLES

TABLE Page

1. INTRODUCTION

The issue of parametric excitation could be of critical importance in the stability analysis of the Deep Water Stable Craneship (DWSC) using time-varying hydrostatics.

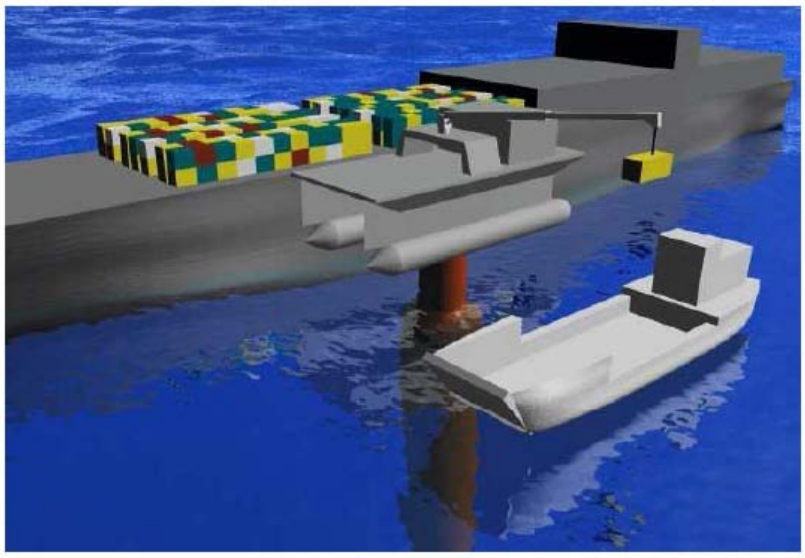

Figure 1. USN's concept of seabasing using the DWSC (Selfridge, 2005).

Parametric or internal excitation occurs in a system when one of the coefficients in the equation of motion (EOM) modeling the system varies with time. Pure parametric excitation results when external forcing is equal to zero. In ocean engineering/ naval architecture, parametric excitation is most often a consequence of time-varying

---

This thesis follows the style of Ocean Engineering.

hydrostatics. Parametric instability might be triggered for certain values of the parameters describing the time-varying coefficient.

The DWSC is comprised of two entities, a stepped classic spar and a catamaran craneship. It was proposed to provide better seakeeping for the United States Navy's seabasing (see Figure 1) goal of transferring containerized cargo between large and small vessels in sea states up to sea state four. Better seakeeping attributes of a spar provide the crane a relatively stable platform, thus minimizing load pendulation.

The DWSC has some unique features, some of which might increase its susceptibility to large motions and parametric instability. They are:

1) the absence of a mooring system: the offshore practice is to permanently moor and physically connect vessels. Multi-vessel dynamic positioning seabase cannot afford the time
2) the absence of strakes: as the DWSC forms a self-deploying, open ocean capable trimaran
3) the absence of heave plates
4) relatively low metacentric height: heave elevation of a stepped classic spar, like the DWSC, is expected to cause a smaller depression of the center of buoyancy B than for a purely classic spar. Hence heave-roll coupling and parametric excitation are supposed to be less significant for the DWSC. On the other hand, with a lower metacentric height GM as compared to spars used in the offshore industry, the heave motion of the DWSC is expected to have a significant influence on the roll EOM.

There are two well-known cases where unfavorable tuning might trigger parametric instability:

1) $T_{n,3} = \frac{1}{2} T_{n,4}$

2) $T_{wave} = \frac{1}{2} T_{n,4}$

Spars are usually designed to avoid the previous two cases. So is the DWSC. However it is important to note that several additional cases of unfavorable tuning are possible. For example, Haslum and Faltinsen (1999) defines

$$T_{critical} = \frac{1}{\frac{1}{T_{n,5}} + \frac{1}{T_{n,3}}} \tag{1.1}$$

This corresponds to the wave frequency which interacts with the natural heave frequency to produce an envelope process with a difference frequency coinciding with the natural pitch frequency.

2. BACKGROUND

A lot of work, both experimental and numerical, has studied the stability and motions of spars in waves. Dern (1972) was one of the first researchers to study the stability of motions of free spars in waves. As a first step he determined the motions from the linearized equations of motion. An approximate wave exciting force acting on the spar was determined using the Froude-Krylov hypothesis. The coefficients appearing in the equations were obtained from model tests. His experiments indicated the presence of a phenomena believed to be of nonlinear origin i.e. rolling in head seas. Therefore Dern introduced nonlinear restoring terms in the equations of motion to explain the phenomena. Dern found linear theory to be valid only if the upper part of the spar is of constant cross section and if it is high enough to avoid over-topping.

It has been known for many years that a ship moving in longitudinal regular waves can perform rolling motions of large amplitude. In 1955, Kerwin explained this motion by the periodic variation of the roll restoring moment due to the on-coming waves. The roll appears as an unstable solution to a Hill's equation. In 1959, Paulling and Rosenberg showed that such instabilities in ship motion could be explained by the effect of second-order coupling terms in the equations of motion.

Haslum and Faltinsen (1999) studied the motion response of spar platforms using a simplified calculation method. The simplified theory was based on a long wavelength

assumption i.e. it assumes no waves were created by the spar. The drag forces on the exterior hull (strakes and cylinder bottom) and the drag effects from the internal structure in the moonpool were calculated using 'Morison' drag elements based on the relative velocity.

They also discussed the heave/pitch coupled Mathieu instability. The time-variation was caused by the influence of the heave motions on the pitch restoring term. This Mathieu instability is general and may occur for all of the spar shapes they presented in Figure 2. The two parameters controlling the pitch restoring term are the submerged volume $\forall$ and the metacentric height GM. If the restoring term is calculated at the displaced position, instead of using the equilibrium position as in linear theory, both $\forall$ and GM are functions of the heave motion. The dominating contributor to static GM is the position of the centre of buoyancy B above the centre of gravity G. The metacentric radius BM is very limited due to a relatively low waterplane area moment of inertia and a large submerged volume.

They concluded that classic cylindrical spars with constant cross section area are vulnerable to vertical excitation at long wave periods due to their low damping and relatively low natural heave periods. They also concluded that large amplitude pitch motions coupled to extreme amplitude heave motions may arise when a spar platform is exposed to regular waves of a particular wave period. This phenomenon was investigated theoretically and explained as a resonance. It was caused by nonlinear coupling effects between heave, surge and pitch. It was shown that for a critical wave

period the envelope of the heave motion makes the pitch motion unstable. Pitch damping may reduce this unstable motion.

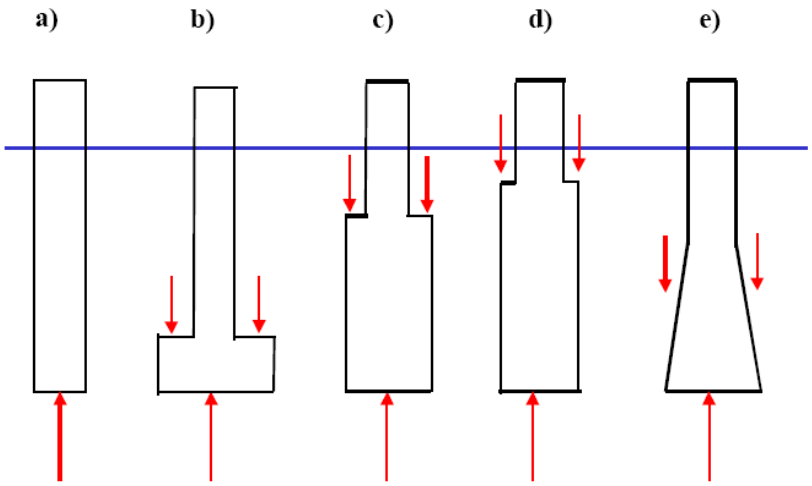

Figure 2. Alternative hull shapes (Haslum and Faltinsen, 1999).

Liao and Yeung (2001) investigated the effects associated with the presence of bilge keels and fluid viscosity on the response near a 'troublesome' resonance condition. Roll response near resonance is strongly affected by viscous damping, not only in terms of the steady state response amplitude, but also in terms of the stability or boundedness of the response itself. They also investigated how the coupled multiple degree of freedom response of a floating body can critically depend on the representation of viscous damping. They showed that the response characteristics were very different depending on whether or not bilge keels and fluid viscosity were considered. For the cylinder with bilge keels, the response showed that the proper modeling of fluid viscosity was critical in order to predict the response accurately. On the other hand,

inviscid fluid models could predict an instability which might not be present in the physical world.

Das and Falzarano (2001) studied the parametric excitation that results when the top of the pontoon of a column stabilized semisubmersible is alternately wetted and dried when a wave passes as the vessel heaves and pitches in head seas. They also investigated the sensitivity of the parametric instability to the representation of the radiated wave force. They specifically compared an approximate constant coefficient representation of the radiated wave force to the more accurate impulse response function representation.

Zhang et al. (2002) studied the instability of the Mathieu's equation with damping using the infinite determinant and the harmonic balance method. General stability diagrams (including damping effects) were generated in a relevant parametric plane to detect the instability zones. It was shown in the stability diagrams that higher-order unstable regions are more sensitive to damping than the lower-order ones. Therefore lower-order unstable regions must be carefully examined and evaluated. It is to be noted that Haslum and Faltinsen (1999) showed a stability diagram for Mathieu's equation ignoring pitch damping effects.

It was shown that the maximum heave motions were very sensitive to heave damping in long wave swells. The major contributions to heave damping were the mooring lines and risers coupled with the riser supports inside the moonpool. Coupled analysis including the aforementioned effects are needed to estimate heave damping accurately. It is to be noted that the heave damping is motion amplitude dependent.

Rho et al. (2002) studied the heave and pitch motions of a spar platform with damping plate, both experimentally and numerically. In experiments in regular waves, they observed that pitch motions are triggered when the magnitude of heave motion exceeds a certain threshold, when the natural pitch period is approximately double the heave natural period. They mentioned typical natural periods of the spars deployed in the Gulf of Mexico to be 160 s for surge, 60 s for pitch and 28 s for heave.They found that the numerical result of heave response at resonance is over-predicted because potential flow theory computer codes underestimate the damping.

Falzarano et al. (2003) explained the method of analyzing stability using Strutt-Ince diagrams. The Strutt-Ince diagram has many advantages. The main advantage is that it allows easy visualization of the change in stability characteristics as parameters are changed.

When a system is parametrically excited the response frequency is typically a sub-harmonic of the excitation frequency. Hence a parametrically excited system may exhibit large motion response amplitudes when the excitation frequency is twice the natural frequency. Another factor which can be important in such a stability analysis is the wave encounter frequency of the vessel.

Mathieu's equation is a special case of the Hill's equation. Two methods are available to find the parameter values for instability in the parametric plane. The first is using the perturbation method and the second is using Hill's infinite determinant.

Tao et al. (2004) explicitly calculated the viscous damping of spars and incorporated it into their potential flow solution. They calculated the nonlinear viscous

heave damping forces by directly solving the Navier-Stokes equation based on the finite difference method. The wave exciting forces, added-mass and damping were calculated using a well known hydrodynamic software package based on potential flow theory. These two are then combined using an iterative procedure. Tao et al. (2000) had previously demonstrated that for a vertical cylinder in resonant heave the viscous damping forces exhibit different characteristics in different parameter regimes, i.e. the damping force appears to be independent of the amplitude at very small amplitudes of oscillation and is evidently dependent on the motion response as the amplitudes of oscillation increase. Viscous effects tend to dominate over the hydrodynamic damping mechanism around heave resonance and the damping model could be improved by introducing a linearization technique. When the heave amplitude of a spar is small, hydrodynamic damping from the spar hull may be small compared to other effects such as damping from risers and the mooring system. However, as a spar experiences large amplitude heave resonance, which is often excessive to the mooring system and riser integrity, the hydrodynamic damping from the spar hull and its appendages may be crucial in suppressing the heave resonance.

Koo et al. (2004) evaluated the damping effects and hull/ mooring/ riser coupling effects on the principal instability. The wave elevation effect on Mathieu instability was also investigated. Mathieu instability of a practical spar platform was carefully analyzed by a series of systematic simulations and comparisons of many different scenarios. Their results showed that the additional pitch restoring force from buoyancy-cans played an important role in suppressing Mathieu instability.

Due to the motion characteristics of a spar, the sum frequency second-order effect is typically not important and thus is not included in the most motion analyses. The wave-force linear force transfer functions and quadratic force transfer functions were calculated in the frequency-domain and then these forces were converted to the time-domain using the two term Volterra series expansion. The frequency-dependent radiation damping was included in the form of a convolution integral in the time-domain simulations. To evaluate the heave and pitch damping ratios and natural periods, free decay simulations were conducted. The results showed that most of the heave damping in a classic spar platform comes from the mooring lines.

When a spar exhibits Mathieu instability, it experiences a lock-in phenomena in the pitch motion. Their results showed that mooring line and riser buoyancy-can effects played an important role in the Mathieu instability analysis by increasing damping and shifting the natural pitch period. Their simulation results showed that the wave elevation effect can be very important for large wave elevations and large phase differences between wave elevations and heave motions.

It is to be noted that Haslum and Faltinsen (1999), Zhang et al. (2002) and Rho et al. (2002) did not consider the effects of time-varying submerged volume. In Haslum's and Rho's studies, the hull/ mooring/ riser coupling effects were not considered. In Koo's study, both were included. In Haslum's and Rho's experiments, the spar models had relatively smaller KBs (i.e. distance between keel and center of buoyancy) compared to real spar platforms. Koo et al. considered a practical spar platform design.

3. PHYSICAL SYSTEM MODELING

3.1. Basis

The spar considered by Selfridge (2005) is used as a basis for modeling the DWSC. Table 1 lists the main dimensions of the DWSC.

Table 1. DWSC's main dimensions.

Dimension	
Length	129.60 m
Draft	118.00 m
Lower section length	113.36 m
Upper section length	4.64 m
Lower section diameter	8.50 m
Upper section diameter	6.00 m
Total displacement	6761.00 t
Center of buoyancy, KB	57.86 m
Center of gravity, KG	56.30 m
Metacentric height, GM	1.57 m
Natural heave period, $T_{n,3}$	30.5 s
Natural pitch period, $T_{n,5}$	148.8 s

3.2. Degrees of freedom

Motions of floating bodies are inherently coupled and the DWSC is no different. Head seas is the only condition considered in this thesis. In head seas surge is coupled to pitch and sway to roll. For small rotations, the parameters controlling the roll stiffness are the submerged volume ∀ and the metacentric height GM. When time-varying hydrostatics are considered, both ∀ and GM are affected by the heave motion (heave motion relative to the mean water line (MWL), to be precise). Therefore for time-varying hydrostatics, heave couples to sway and roll. However it is to be noted that both sway and roll do not have any direct forcing in head seas. Also between sway and roll, only roll has restoring forces. Roll is therefore susceptible to resonant motions. The possibility and susceptibility to resonant roll motions in head seas makes the investigation of parametric roll crucial. In addition to looking at coupled heave-sway-roll motions, interesting insight might be gained by decoupling the roll EOM from the other degrees of freedom (DOF). Decoupling the roll EOM from the other DOF requires the determination of the ‘roll center’. The inertial, damping and stiffness coefficients then need to be determined about this new coordinate system center. In this thesis, instead of decoupling the roll EOM from the other DOF, the single DOF roll EOM about the MWL is used for the stability analysis. A single DOF roll EOM is amenable to the kind of stability analysis typically performed and carried out in this thesis.

3.3. Single degree of freedom roll motion

The heave-roll coupling can be represented by Mathieu's or Hill's equation. Roll motion in head seas is an unstable solution to Mathieu's or Hill's equation. The single DOF roll EOM that is used to model the DWSC is given by equation 3.1.

$$(I_{44} + A_{44}(\omega_n))\frac{d^2\phi}{dt^2} + B_{44}(\omega_n)\frac{d\phi}{dt} + \Delta GZ(\phi,t) = 0 \tag{3.1}$$

It is to be noted that the single DOF roll oscillator described by equation 3.1 vibrates at the damped natural frequency, which is only slightly different from the undamped natural frequency. Therefore ω_n is used in equation 3.1.

Mathieu's equation (equation 3.2), a special case of Hill's equation (equation 3.3), is a second-order ordinary differential equation with a harmonic coefficient.

$$\frac{d^2\phi}{dt^2} + 2\mu\frac{d\phi}{dt} + (a + 16q\cos 2t)\phi = 0 \tag{3.2}$$

$$\frac{d^2\phi}{dt^2} + 2\mu\frac{d\phi}{dt} + (\theta_0 + \mu^2 + 2\sum_{\nu=1}^{\infty}\theta_\nu \cos 2\nu t)\phi = 0 \tag{3.3}$$

The righting arm $GZ(\phi,t)$ is seen to be a function of both time and angle of roll. However in this thesis the variation of GM is modeled instead of $GZ(\phi,t)$. For small angles, $GZ(\phi,t)$ can be linearly approximated by $GM(t)\phi$. Therefore equation 3.1 reduces to

$$(I_{44} + A_{44}(\omega_n))\frac{d^2\phi}{dt^2} + B_{44}(\omega_n)\frac{d\phi}{dt} + \Delta GM(t)\phi = 0 \tag{3.4}$$

$\Delta GM(t)$ in this thesis is modeled as

$$\Delta GM(t) = C_{44}(t) = \forall(t)\rho g GM(t) \tag{3.5}$$

where

$$GM(t) = KB(t) + BM(t) - KG \tag{3.6}$$

and

$$BM(t) = \frac{I(t)}{\forall(t)} \tag{3.7}$$

where $I(t)$ is either of two values, depending on A_{wp}

Substituting in equation 3.5, equation 3.4 further reduces to

$$(I_{44} + A_{44}(\omega_n))\frac{d^2\phi}{dt^2} + B_{44}(\omega_n)\frac{d\phi}{dt} + C_{44}(t)\phi = 0 \tag{3.8}$$

3.4. Coupled heave-sway-roll motion

The heave EOM can be solved independently of the sway and roll EOM. In this thesis it is solved both ignoring and considering viscous drag. The heave EOM with viscous drag can be written as

$$(M_{33} + A_{33}(\omega))\frac{d^2\xi_3}{dt^2} + B_{33}(\omega)\frac{d\xi_3}{dt} + C_{33}(t)\xi_3 = F_3(\omega,t) + F_{D,upper}(t) + F_{D,lower}(t) \tag{3.9}$$

where $C_{33}(t)$ is either of two values, depending on A_{wp}

$$C_{33} = A_{wp}\rho g \tag{3.10}$$

C_{33} is a function of t as it depends on where the waterline is (which in turn depends on the relative heave). It is important to note that there are two horizontal surfaces (one circular, the other annular) for the viscous drag to act on. The viscous heave drag in this thesis has been incorporated in a rather nonlinear fashion: the distances of the horizontal surfaces from the instantaneous waterline are taken into account. For instance, if the

lower section of the DWSC penetrates the water surface, zero viscous drag is calculated to act on the upper horizontal surface (i.e. the annulus).

The concept of relative heave is defined to account for the effect of wave elevation. Relative heave is the heave of the DWSC w.r.t. the instantaneous waterline. Therefore it is the relative heave which is coupled to the sway and roll EOM.

$$\xi_{3,relative} = \xi_3 - \eta \tag{3.11}$$

It is assumed above that the wave profile is such that the waterplane area can be considered a horizontal surface.

Once the heave EOM is solved for, the sway and roll EOM are solved together without and with viscous drag. The sway and roll EOM with viscous drag are as follows

$$(M_{22} + A_{22}(\omega))\frac{d^2\xi_2}{dt^2} + (M_{24} + A_{24}(\omega))\frac{d^2\xi_4}{dt^2} + B_{22}(\omega)\frac{d\xi_2}{dt} + B_{24}(\omega)\frac{d\xi_4}{dt} = F_{2,D}(t) \tag{3.12}$$

$$(M_{42} + A_{42}(\omega))\frac{d^2\xi_2}{dt^2} + (M_{44} + A_{44}(\omega))\frac{d^2\xi_4}{dt^2} + B_{42}(\omega)\frac{d\xi_2}{dt} + B_{44}(\omega)\frac{d\xi_4}{dt} + C_{44}(t)\xi_4 = F_{4,D}(t) \tag{3.13}$$

The sways and roll viscous drag is calculated using ‘Morison’ drag elements based on relative velocity. It is to be noted that in this thesis four ‘Morison’ drag elements have been used. Also, only elements till the mean waterline are considered.

The same C_D is used for both the horizontal surfaces. In this thesis, following Chakrabarti (2005), $C_{D,h}$ = 1.2 (C_D for horizontal surfaces) and $C_{D,v}$ = 0.6 (C_D for vertical surfaces).

4. PROBLEM ANALYSIS TECHNIQUE

4.1. General

The main result of this thesis is that due to relative heave motion both ∀ and GM of the DWSC change with time. This couples the sway and roll EOM to relative heave. Also, the heave-roll coupling (neglecting the sway EOM) allows the use of Mathieu's equation for stability analysis.

However it is important to understand that the Strutt-Ince diagram (stability diagram)s only requires the determination of $C_{44}(t)$ and its consequent Fourier analysis. The advantages of using the Strutt-Ince diagram for stability analysis will be discussed soon.

The capability to simulate the sway and roll EOM helps in verifying the stability analysis and allows one to see the effect that viscous damping has. Available damping is known to be important in suppressing any instability. Therefore simulating the sway and roll EOM allows for an accurate evaluation of available damping and its effect on containing parametric instability.

4.2. First step

As a first step the hydrodynamic analysis of the DWSC was carried out using WAMIT (Wave Analysis MIT) 6.414. WAMIT 6.414 is a panel method computer program based on linear potential flow theory. It provides, amongst other things, added-

mass and damping coefficients, exciting forces and RAOs. The hydrodynamic analysis carried out for this thesis has the following features:

1) single body analysis
2) infinite water depth
3) irregular frequency removal
4) exciting force from diffraction potential

4.3. Stability analysis background

The determination of $C_{44}(t)$ for the DWSC is done by numerical simulation using MATLAB (Matrix Laboratory). It is carried out both without and with viscous drag. $C_{44}(t)$ is used in the stability analysis in the following manner. Fourier analysis is done on $C_{44}(t)$ to get its first harmonic δC_{44}. For stability analysis using Mathieu's equation, equation 3.8 is further simplified by assuming

$$C_{44}(t) = C_{44,mean} + \delta C_{44}\cos(\omega t) \tag{4.1}$$

Following the method employed by Das (2000) and Francescutto (2001), equation 4.1 yields

$$\frac{d^2\phi}{dt^2} + \frac{2}{\omega}\frac{B_{44}(\omega_n)}{(I_{44} + A_{44}(\omega_n))}\frac{d\phi}{dt} + 4\frac{\omega_n^{\,2}}{\omega^2}(1 + \frac{\delta C_{44}}{C_{44,mean}}\cos(2t))\phi = 0 \tag{4.2}$$

The above equation is compared to equation 3.2. By equating like terms, the following is deduced

$$2\mu = \frac{2}{\omega}\frac{B_{44}(\omega_n)}{(I_{44} + A_{44}(\omega_n))} \tag{4.3}$$

$$a = 4\frac{\omega_n^{\,2}}{\omega^2} \tag{4.4}$$

$$16q = 4\frac{\omega_n^{\,2}}{\omega^2}\frac{\delta C_{44}}{C_{44,mean}} \tag{4.5}$$

Only the first unstable zone is investigated in this thesis. This is because considerable wave energy is at wave periods much lesser than $\frac{1}{2}T_{n,4}$. Equations 4.3, 4.4 and 4.5 are used to plot the points corresponding to the stability states of the DWSC onto the Strutt-Ince diagram.

The Strutt-Ince diagram used in this thesis is drawn on the $a-q$ plane. For generating the first unstable zone of the Strutt-Ince diagram, the following relations from Hayashi (1964) are used. They are defined w.r.t equation 3.2.

$$a = 1 + 8q\cos 2\sigma + q^2(-16 + 8\cos 4\sigma) - 8q^3\cos 2\sigma \tag{4.6}$$

$$\mu = 4q\sin 2\sigma - 12q^3\sin 2\sigma \tag{4.7}$$

where μ is the non-dimensional damping ratio. For every μ, a set of pairs (a,q) defines the boundary of the stability/ instability region. Any point lying above this boundary corresponds to an instability state for that particular μ. Similarly any point lying below that boundary corresponds to a stability state for that particular μ.

Therefore the Strutt-Ince diagram plots the stability/ instability domain as a function of inverse frequency ratio (where frequency ratio = $\frac{\omega}{\omega_n}$) and relative excitation (see equations 4.4 and 4.5).

It is to be noted that with increasing damping ratios the unstable region reduces in size and moves further away from the horizontal axis.

Stability analysis using the Strutt-Ince diagram has the following advantages:

1) allows easy visualization of the change in stability as parameters are varied
2) multiple physical situations can be compared at the same time
3) can be very useful in design

4.4. Simulation background

Time simulations are done for a monochromatic wave i.e. only regular waves are considered in this thesis. Therefore the hydrodynamic coefficients can be assumed to be constant in this analysis. The simulations use the ode45 solver (based on Runge-Kutta (4,5) formula) to solve ξ_3 first. Then ξ_2 and ξ_4 are solved for.

5. RESULTS

5.1. Format of results

The results presented in this thesis are primarily organized according to the structure analyzed and secondarily according to the method of analysis. Two structures viz. the DWSC and a modified DWSC are analyzed to different extents. Frequency-domain, time-domain, Fourier and stability analysis are employed. The secondary organization is discarded for the modified DWSC. This omission helps to highlight the influence of viscous drag on a parametrically excited system in a more deliberate fashion.

A modified DWSC is created to demonstrate the typical characteristics of parametric instability at appropriate tunings. DWSC's I_{44}^{B} was reduced by 60% to arrive at the modified DWSC configuration. Such a structure does not seem to be 'realistic'.

Frequency-domain results are obtained from WAMIT. Time-domain simulations are from a suite of programs written in MATLAB. These programs utilize WAMIT's frequency-domain output. Fourier analysis is carried out to identify the first harmonic of $C_{44}(t)$. Stability analysis then yields the stability state corresponding to physical situations.

Wave periods are chosen for either of two reasons: to investigate the behavior of the DWSC in certain sea states or to investigate certain critical phenomena. Sea states two through four are studied as the DWSC was conceptualized to increase operational

limits from sea state two to sea state four. Sea states five and eight are studied to gain insight into the DWSC's behavior at higher 'survival' sea states. Wave periods range from 4.2 s to 34.5 s. The possibility and probability of existence of longer waves with respect to this range are a matter of debate. Wave amplitudes for waves corresponding to the sea states considered are taken as half the mean significant wave height of the respective sea states. They range from 0.15 m to 5.75 m.

5.2. DWSC: frequency-domain

Figure 3 show the heave wave exciting force vs. wave frequency for the DWSC. An area of special interest with respect to the heave wave exciting force is magnified into in Figure 4. In Figure 5 the pitch RAOs for the DWSC and a modified DWSC are presented.

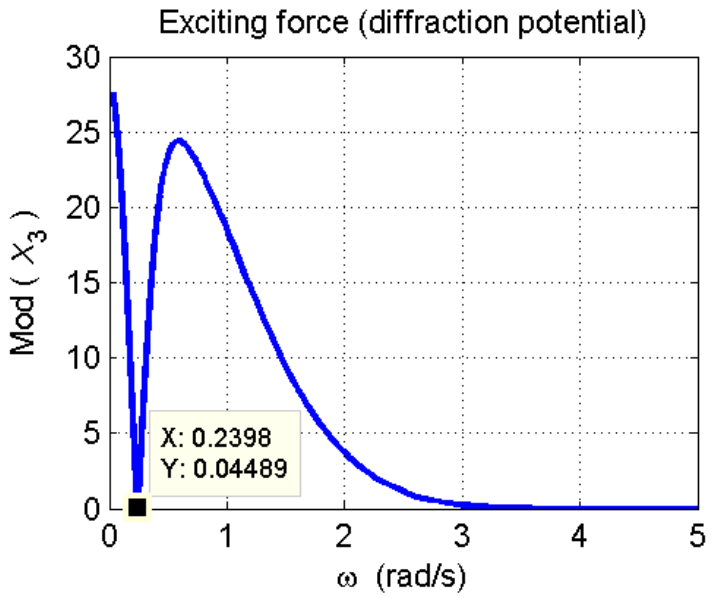

Figure 3. Heave wave exciting force vs. wave frequency for the DWSC.

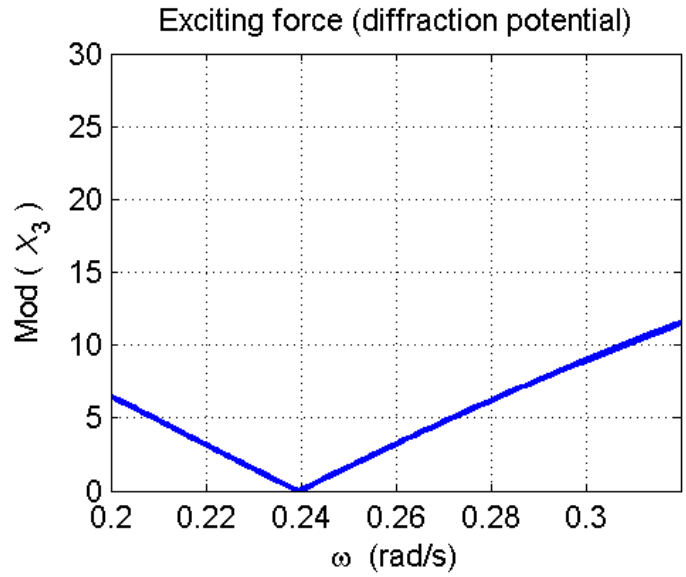

Figure 4. Heave wave exciting force vs. wave frequency for the DWSC (magnified).

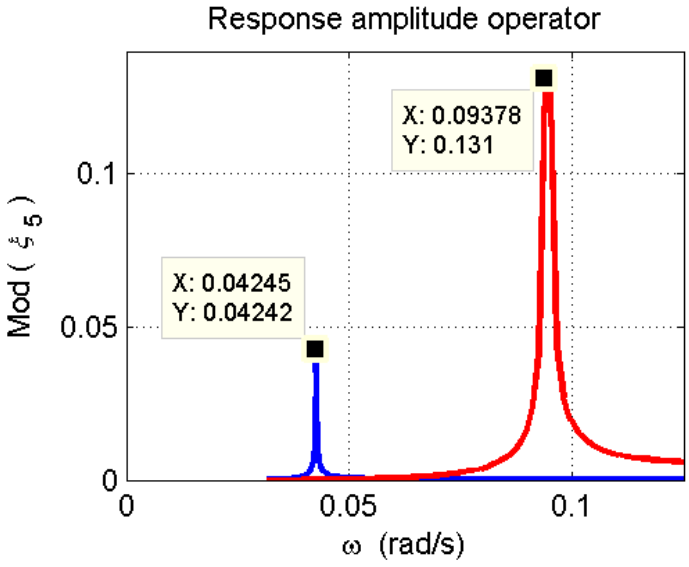

Figure 5. Pitch RAO for the DWSC and a modified DWSC.

5.3. DWSC: time-domain simulations

Time histories of C_{44} ignoring and considering viscous drag are presented in increasing order of sea state and then wave period. Then time histories of ξ_3, ξ_2 and ξ_4 ignoring and considering viscous drag for $T_{wave} = T_{critical}$ are presented.

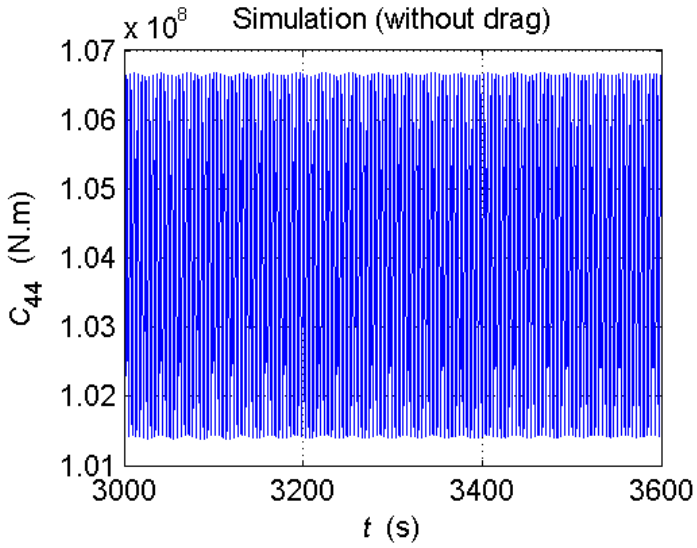

Figure 6. Roll stiffness variation: $T_{wave} = 4.2$ s and $A = 0.15$ m (sea state 2).

Figures 6-23 show the roll stiffness time histories ignoring and considering viscous heave drag for regular waves corresponding to sea states two through four. Figures 6, 8, 10, 12, 14, 16, 18, 20 and 22 show the roll stiffness time histories ignoring viscous drag. Figures 7, 9, 11, 13, 15, 17, 19, 21 and 23 show the roll stiffness time histories considering viscous drag. Figures 24 and 25 show the roll stiffness time histories ignoring and considering viscous drag for $T_{wave} = T_{critical}$.

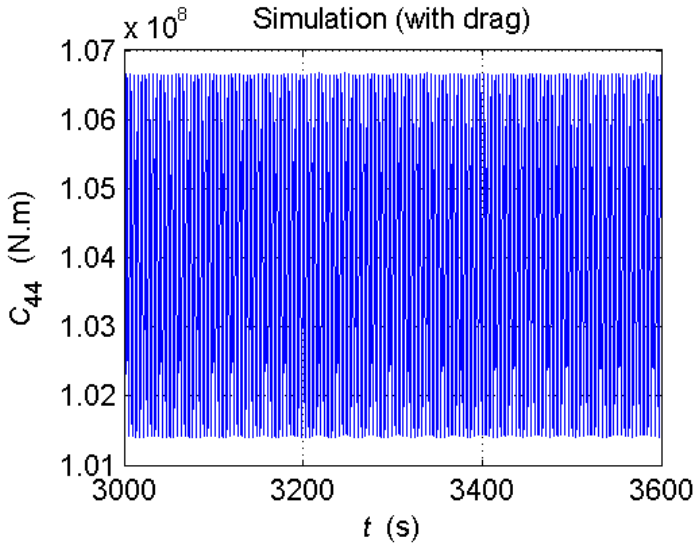

Figure 7. Roll stiffness variation (drag) : $T_{wave} = 4.2$ s and $A = 0.15$ m (sea state 2).

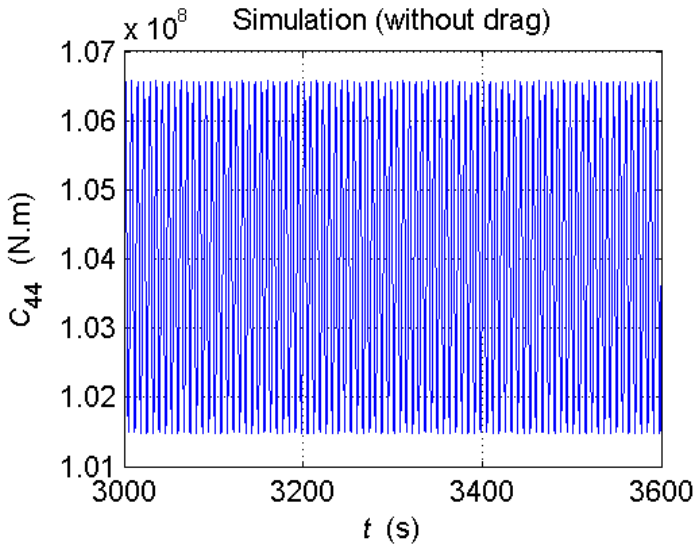

Figure 8. Roll stiffness variation: $T_{wave} = 6.9$ s and $A = 0.15$ m (sea state 2).

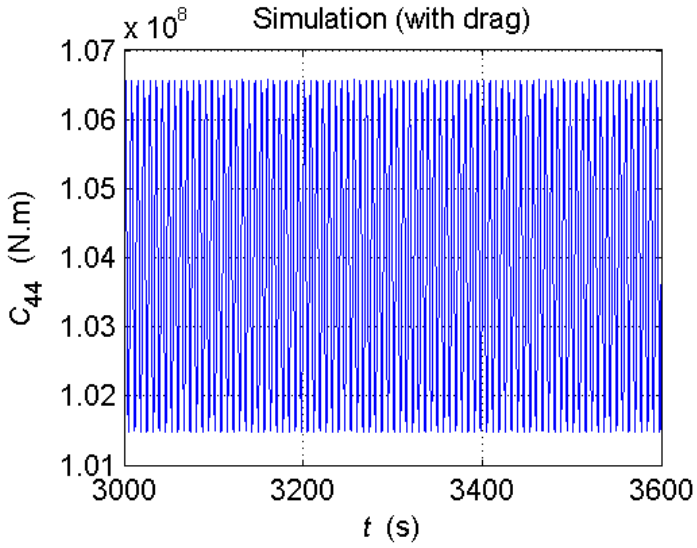

Figure 9. Roll stiffness variation (drag) : $T_{wave} = 6.9$ s and $A = 0.15$ m (sea state 2).

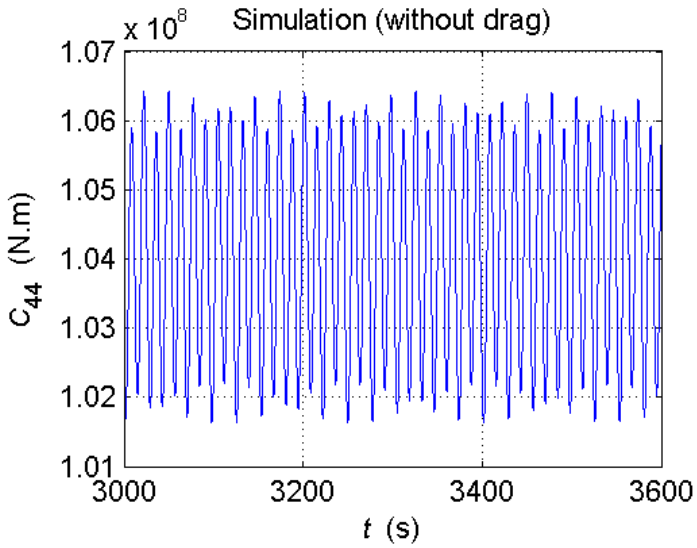

Figure 10. Roll stiffness variation: $T_{wave} = 13.8$ s and $A = 0.15$ m (sea state 2).

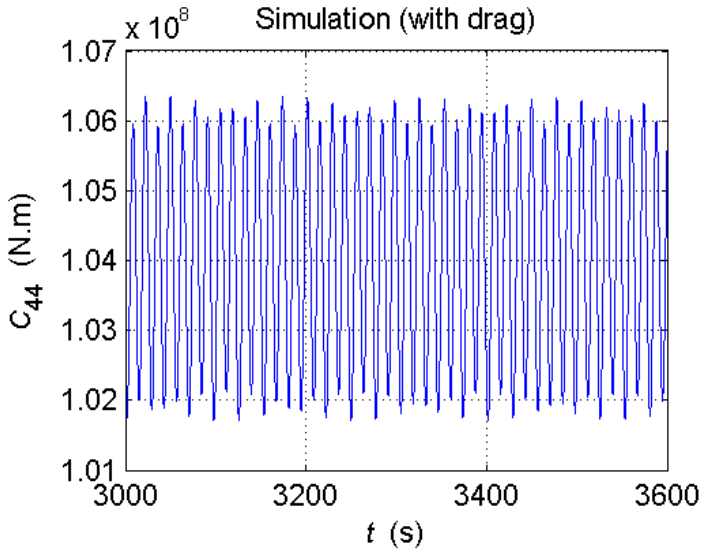

Figure 11. Roll stiffness variation (drag) : $T_{wave} = 13.8$ s and $A = 0.15$ m (sea state 2).

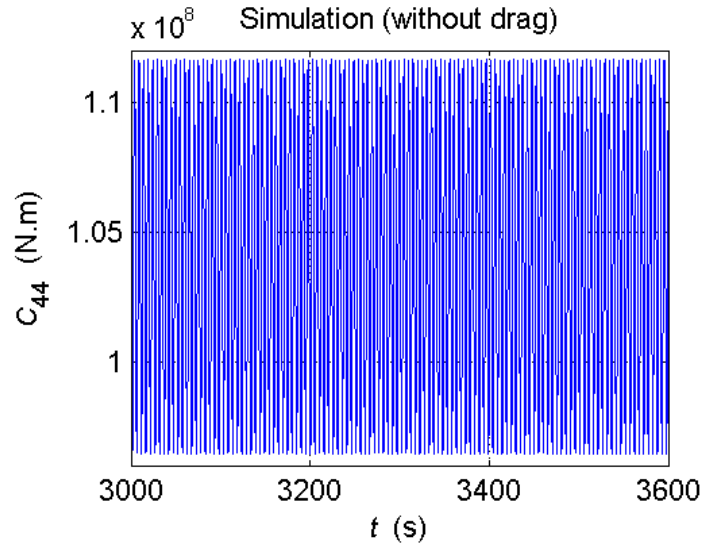

Figure 12. Roll stiffness variation: $T_{wave} = 5.1$ s and $A = 0.4375$ m (sea state 3).

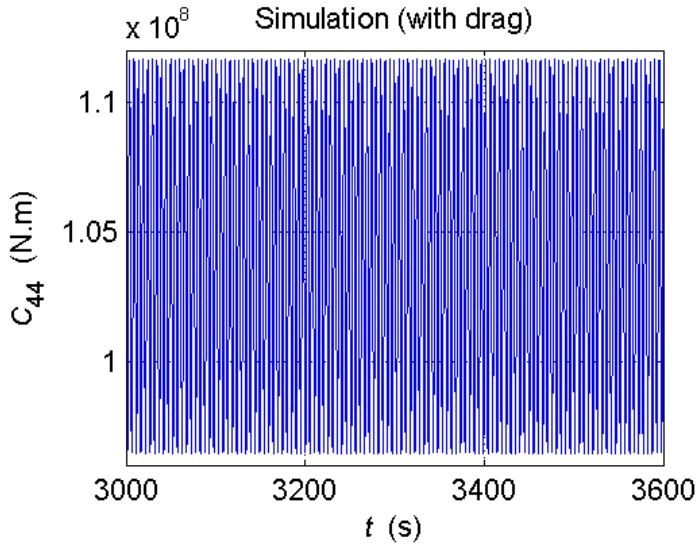

Figure 13. Roll stiffness variation (drag) : $T_{wave} = 5.1$ s and $A = 0.4375$ m (sea state 3).

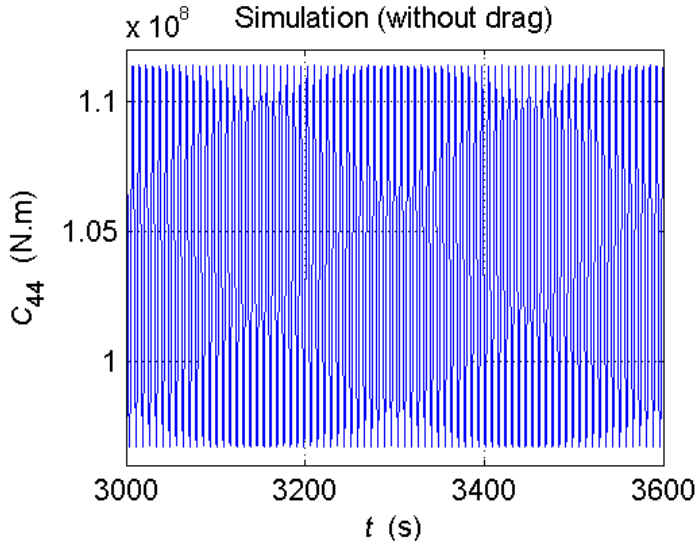

Figure 14. Roll stiffness variation: $T_{wave} = 7.5$ s and $A = 0.4375$ m (sea state 3).

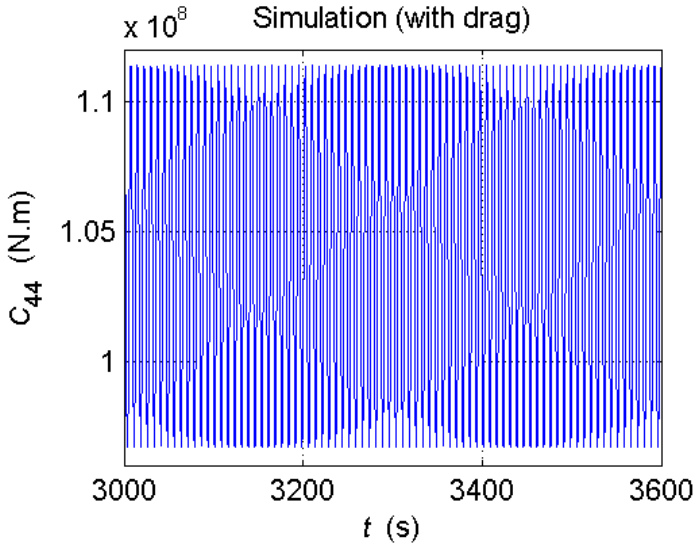

Figure 15. Roll stiffness variation (drag) : $T_{wave} = 7.5$ s and $A = 0.4375$ m (sea state 3).

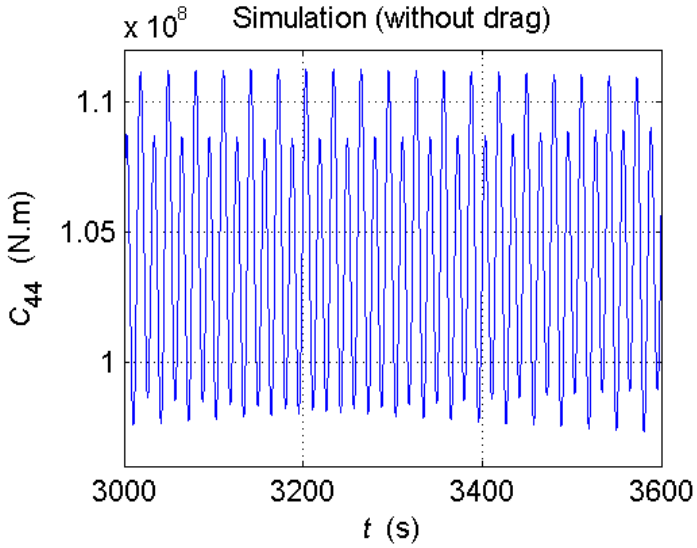

Figure 16. Roll stiffness variation: $T_{wave} = 15.4$ s and $A = 0.4375$ m (sea state 3).

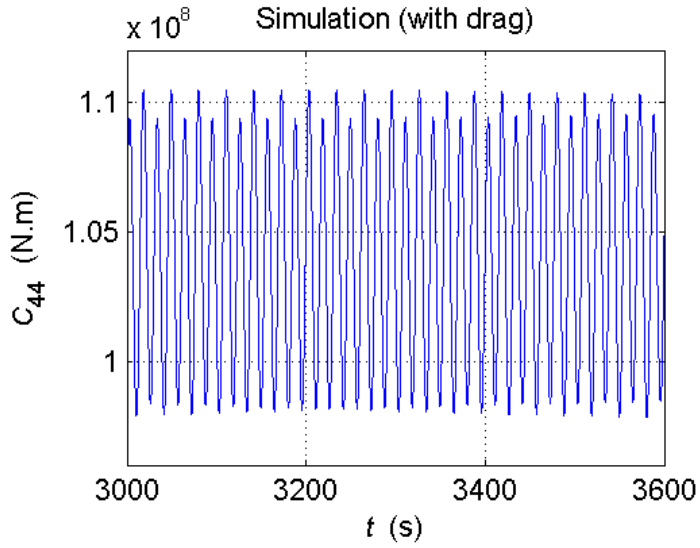

Figure 17. Roll stiffness variation (drag) : $T_{wave} = 15.4$ s and $A = 0.4375$ m (sea state 3).

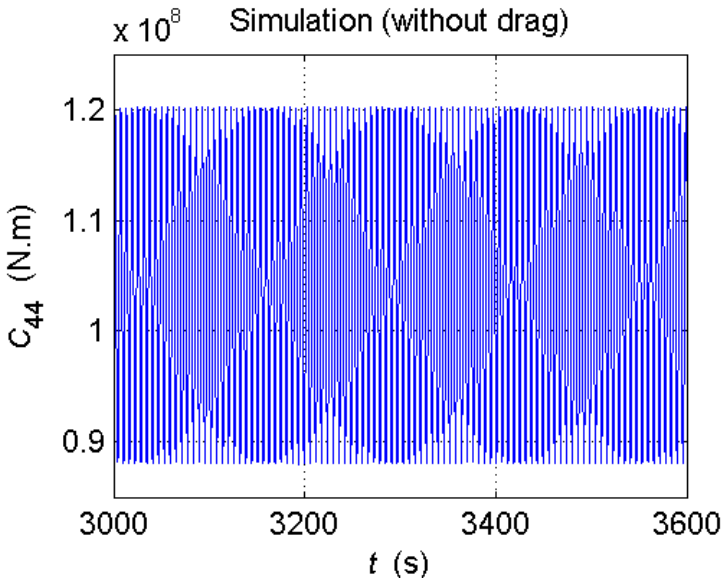

Figure 18. Roll stiffness variation: $T_{wave} = 6.1$ s and $A = 0.9375$ m (sea state 4).

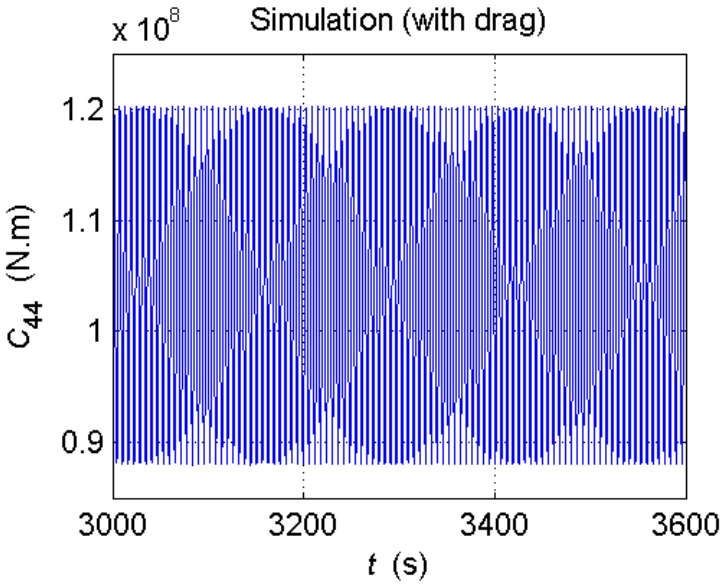

Figure 19. Roll stiffness variation (drag) : $T_{wave} = 6.1$ s and $A = 0.9375$ m (sea state 4).

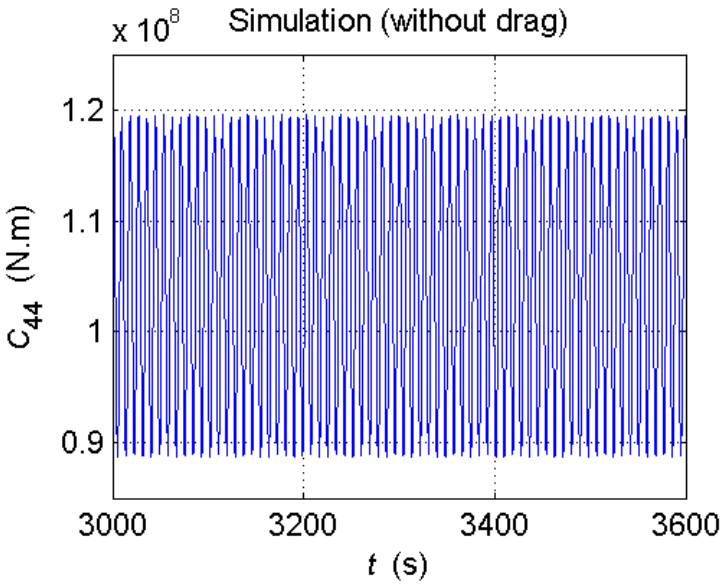

Figure 20. Roll stiffness variation: $T_{wave} = 8.8$ s and $A = 0.9375$ m (sea state 4).

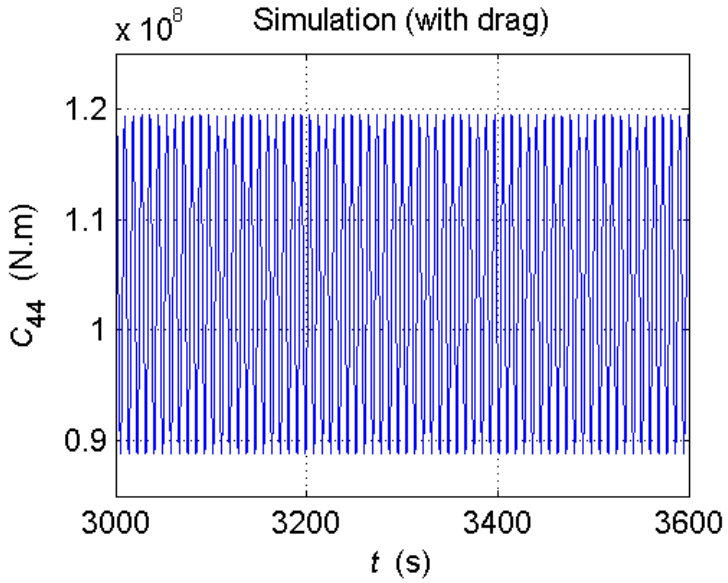

Figure 21. Roll stiffness variation (drag) : $T_{wave} = 8.8$ s and $A = 0.9375$ m (sea state 4).

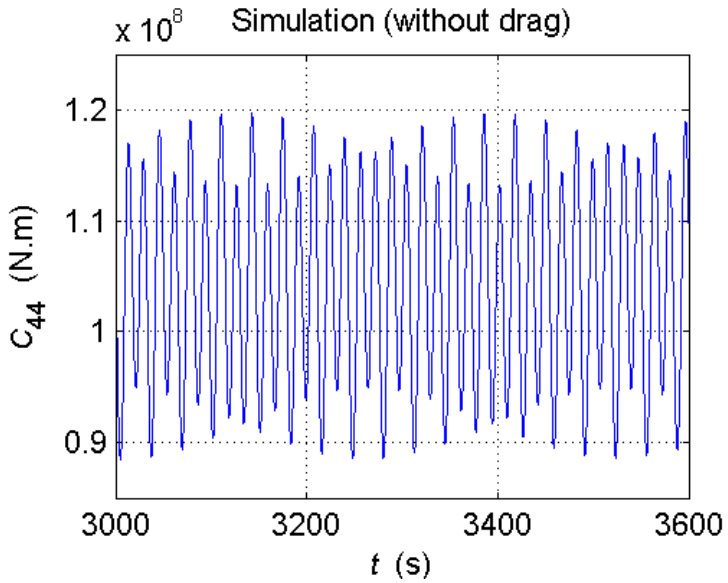

Figure 22. Roll stiffness variation: $T_{wave} = 16.2$ s and $A = 0.9375$ m (sea state 4).

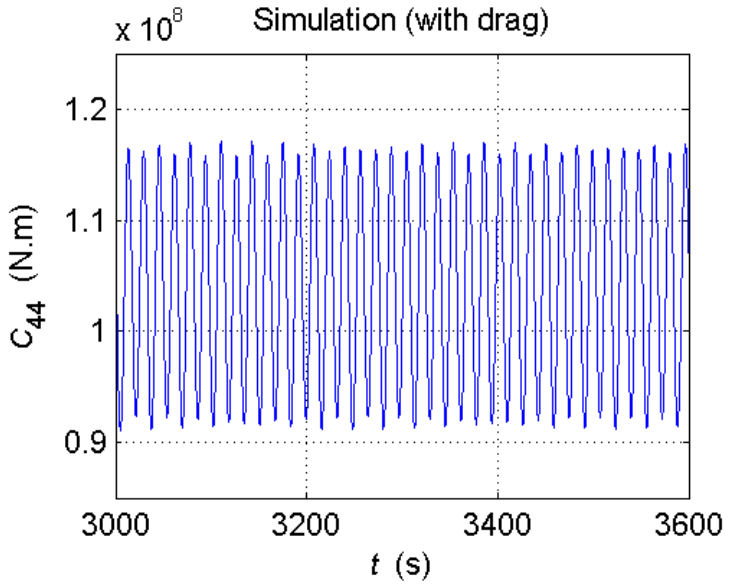

Figure 23. Roll stiffness variation (drag) : $T_{wave} = 16.2$ s and $A = 0.9375$ m (sea state 4).

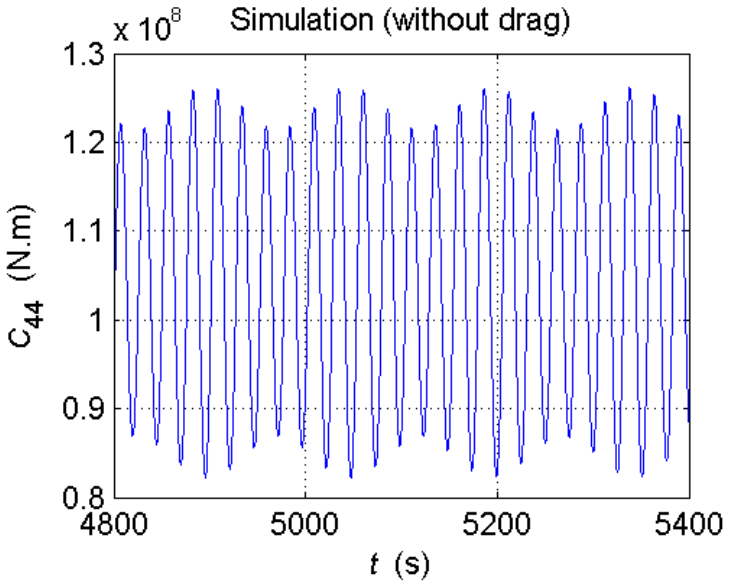

Figure 24. Roll stiffness variation: $T_{wave} = T_{critical}$ and $A = 1.25$ m.

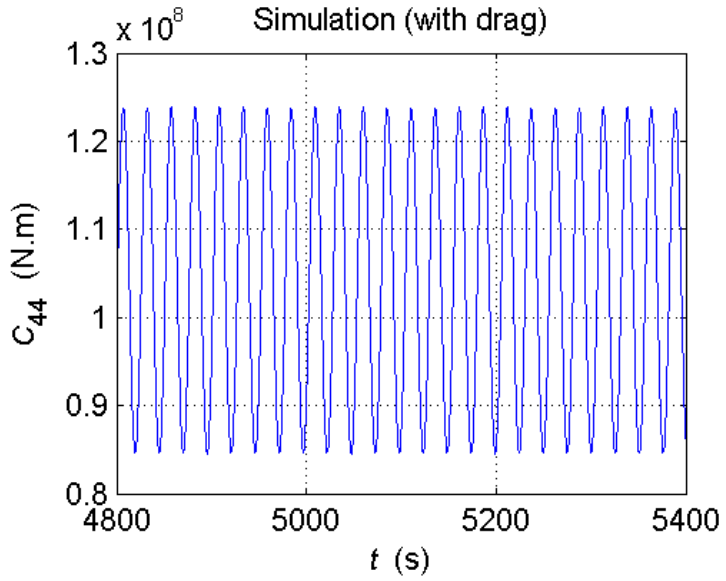

Figure 25. Roll stiffness variation (drag) : $T_{wave} = T_{critical}$ and $A = 1.25$ m.

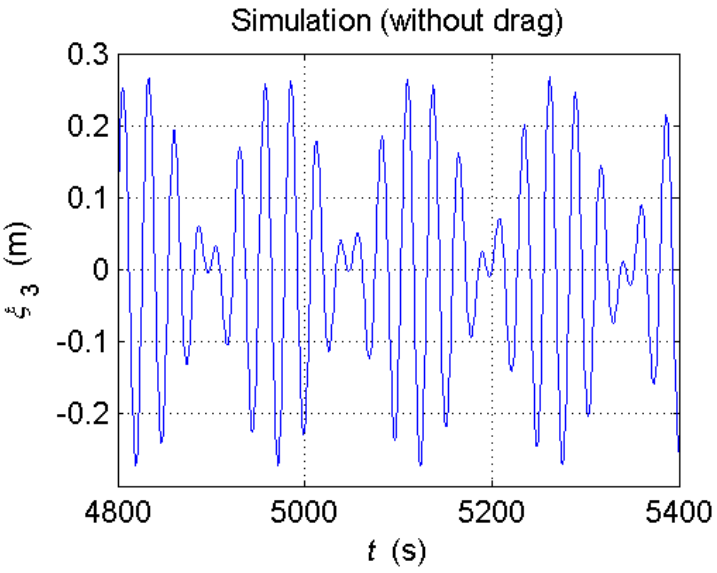

Figure 26. Heave displacement variation: $T_{wave} = T_{critical}$ and $A = 1.25$ m.

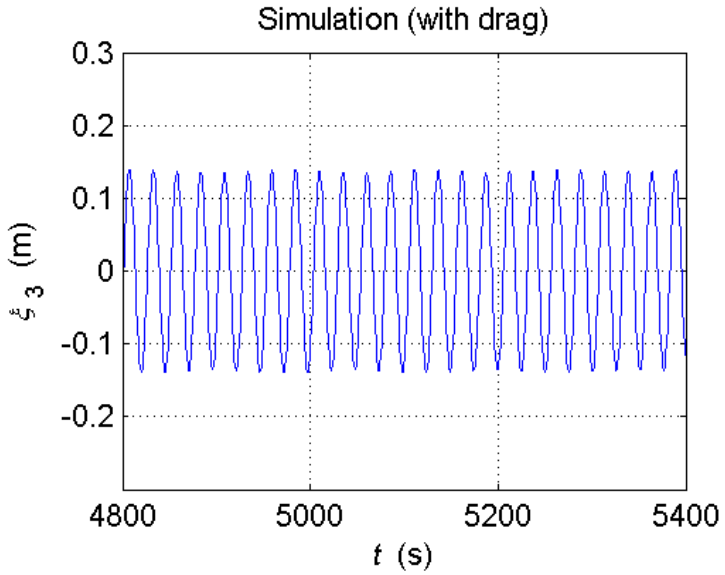

Figure 27. Heave displacement variation (drag) : $T_{wave} = T_{critical}$ and $A = 1.25$ m.

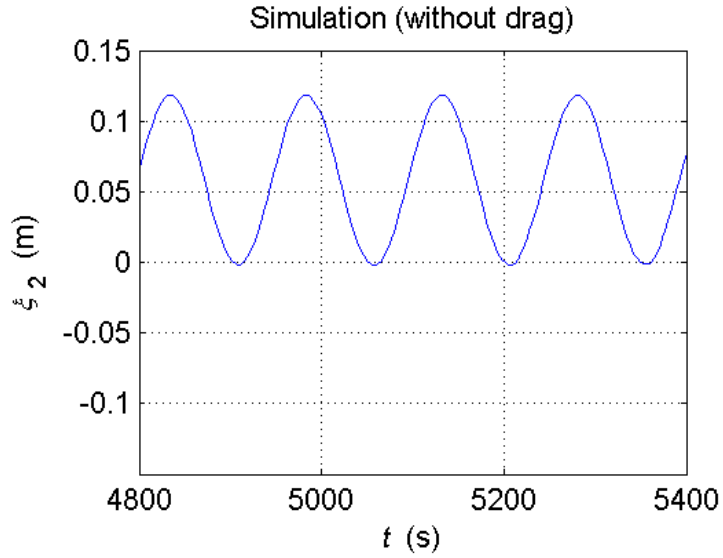

Figure 28. Sway displacement variation: $T_{wave} = T_{critical}$ and $A = 1.25$ m.

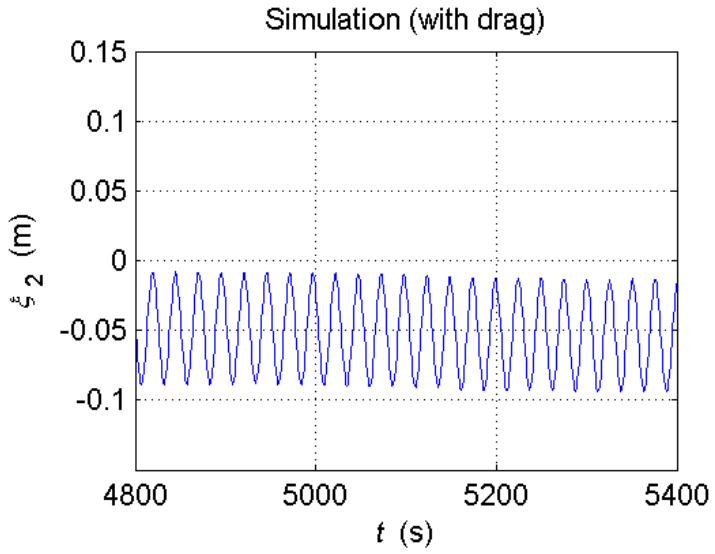

Figure 29. Sway displacement variation (drag) : $T_{wave} = T_{critical}$ and $A = 1.25$ m.

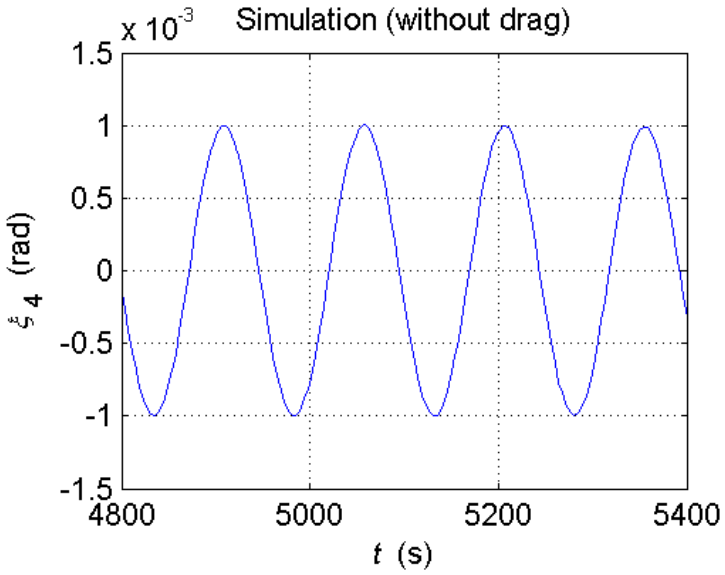

Figure 30. Roll displacement variation: $T_{wave} = T_{critical}$ and $A = 1.25$ m.

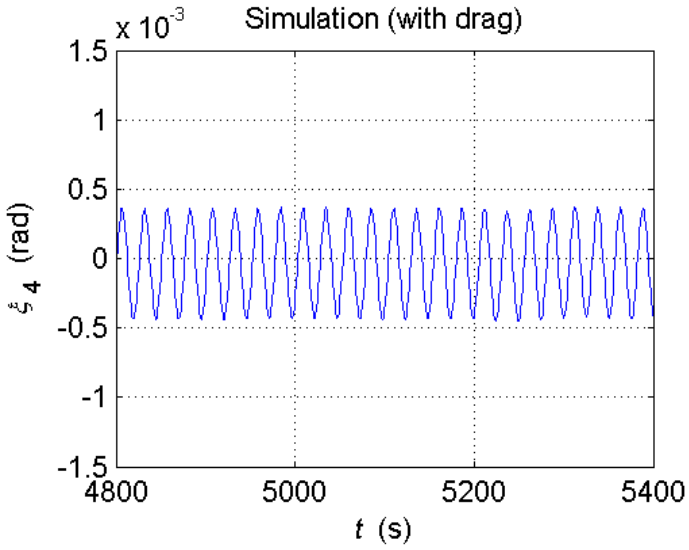

Figure 31. Roll displacement variation: $T_{wave} = T_{critical}$ and $A = 1.25$ m.

Time histories of heave displacement ξ_3 ignoring and considering viscous drag for $T_{wave} = T_{critical}$ are presented in Figures 26 and 27. Figures 28 and 29 show the time histories of sway displacement ξ_2 ignoring and considering viscous drag for $T_{wave} = T_{critical}$. Time histories of roll displacement ξ_4 ignoring and considering viscous drag for $T_{wave} = T_{critical}$ are presented in Figures 30 and 31.

5.4. DWSC: Fourier analysis

Stability analysis using Mathieu's equation requires only the first harmonic of the roll stiffness variation. Time histories of C_{44} ignoring and considering viscous drag are analyzed for its first harmonic using a fast Fourier transform (FFT) algorithm. The ratios of the first harmonics of $C_{44}(t)$ (without viscous drag) to $C_{44,mean}$ are calculated for previously used pairs of wave periods and amplitudes. Table 2 lists the output of the

Table 2. Input data for the stability analysis of the DWSC.

T_{wave} (s)	A (m)	$\delta C_{44,w/o}$ (N.m)	$\delta C_{44,with}$ (N.m)	$\frac{\delta C_{44,w/o}}{C_{44,mean}}$	NATO Sea state
25.31	1.2500	19640000	19620000	0.188680951	n/a
4.20	0.1500	2336000	2336000	0.022441889	2
6.90	0.1500	2475000	2475000	0.023777258	2
13.80	0.1500	2052000	2053000	0.019713509	2
5.10	0.4375	7534000	7534000	0.072378935	3
7.50	0.4375	7310000	7310000	0.070226973	3
15.40	0.4375	5393000	5394000	0.051810406	3
6.10	0.9375	14700000	14700000	0.141222504	4
8.80	0.9375	15000000	15000000	0.144104596	4
16.20	0.9375	11470000	11470000	0.110191981	4
7.20	1.6250	26340000	26340000	0.253047671	5
9.70	1.6250	24650000	24650000	0.236811886	5
16.60	1.6250	20850000	20850000	0.200305389	5
14.40	5.7500	79110000	78710000	0.760007641	8
16.40	5.7500	71920000	70510000	0.690933504	8
20.00	5.7500	70250000	69270000	0.674889859	8

Fourier analysis. In addition to previously used pairs of wave periods and amplitudes, sea states five and eight are utilized in the Fourier analysis.

5.5. DWSC: stability analysis

The Strutt-Ince diagram is used to predict the stability or instability of a parametrically excited system when the system is modeled by Mathieu's equation. These diagrams are presented in increasing order of sea states and then wave periods (corresponding to pairs of wave periods and amplitudes previously used in time-domain simulations). Figures 32-34 show the Strutt-Ince diagrams corresponding to sea state two. Figures 35-37 show the Strutt-Ince diagrams corresponding to sea state three. Figures 38-40 show the Strutt-Ince diagrams corresponding to sea state four. The Strutt-Ince diagram corresponding to $T_{wave} = T_{critical}$ is presented in Figure 41.

A diagram combining the presented stability states (Figures 32-40) and those corresponding to sea states (SS) five and eight is shown in Figure 42 to highlight

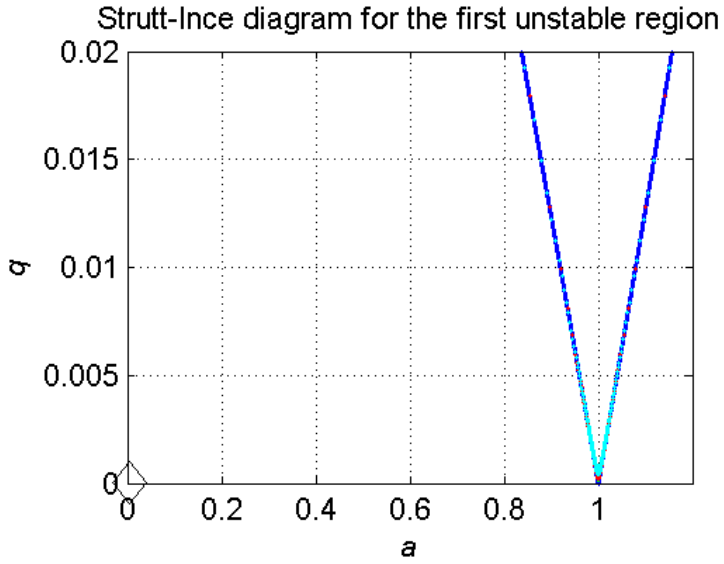

Figure 32. Strutt-Ince diagram: $T_{wave} = 4.2$ s and $A = 0.15$ m (sea state 2).

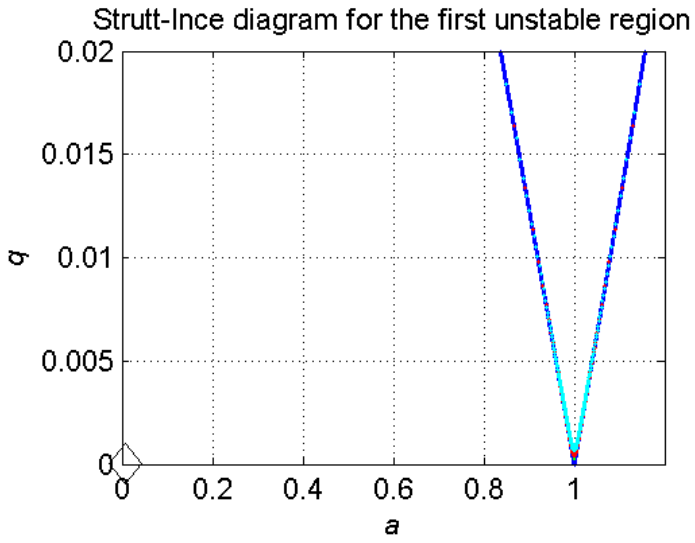

Figure 33. Strutt-Ince diagram: $T_{wave} = 6.9$ s and $A = 0.15$ m (sea state 2).

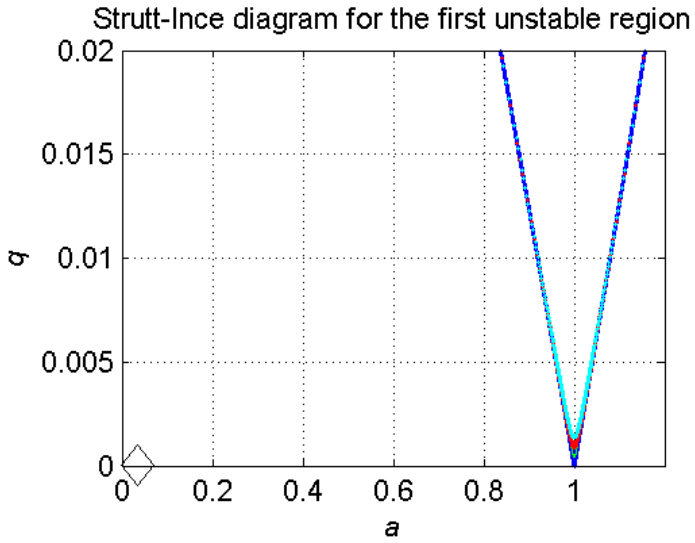

Figure 34. Strutt-Ince diagram: $T_{wave} = 13.8$ s and $A = 0.15$ m (sea state 2).

possible trends in stability with respect to sea states, wave periods and amplitudes.

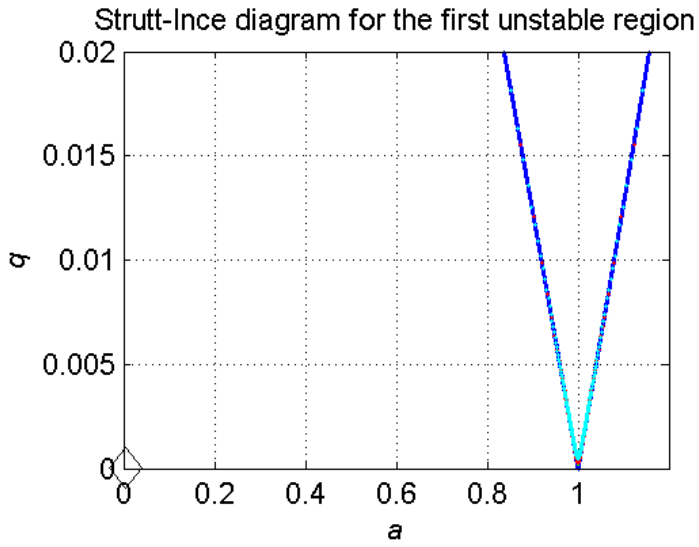

Figure 35. Strutt-Ince diagram: $T_{wave} = 5.1$ s and $A = 0.4375$ m (sea state 3).

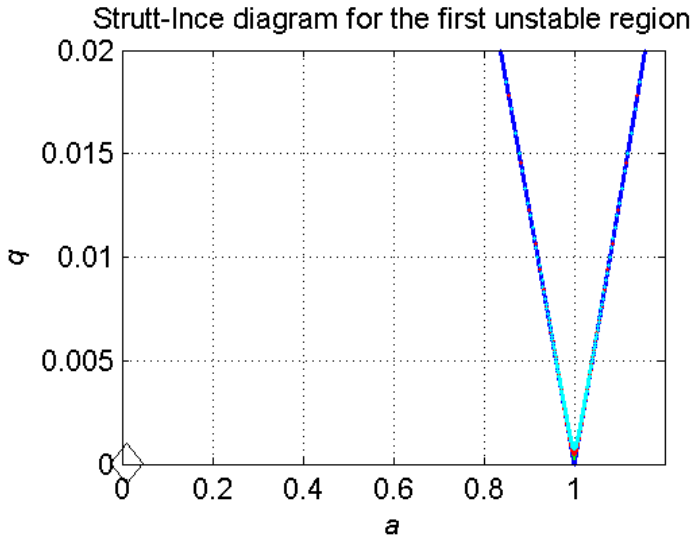

Figure 36. Strutt-Ince diagram: $T_{wave} = 7.5$ s and $A = 0.4375$ m (sea state 3).

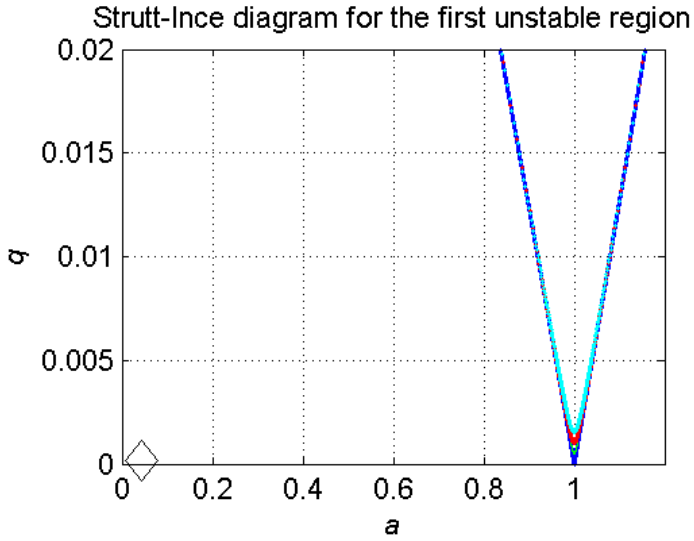

Figure 37. Strutt-Ince diagram: $T_{wave} = 15.4$ s and $A = 0.4375$ m (sea state 3).

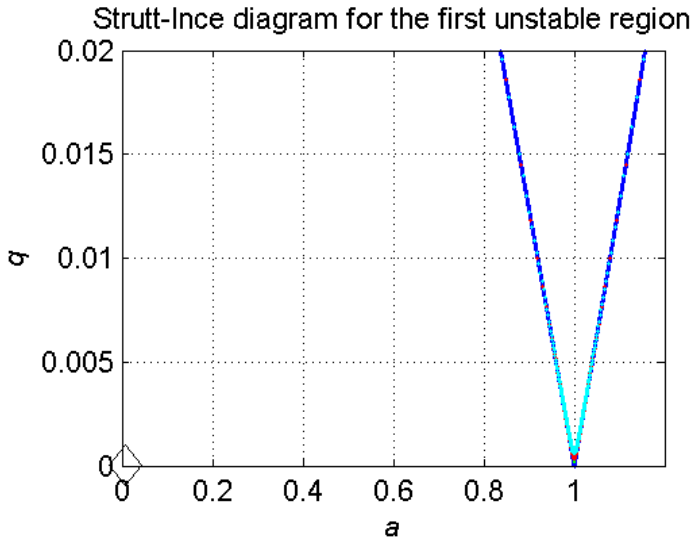

Figure 38. Strutt-Ince diagram: $T_{wave} = 6.1$ s and $A = 0.9375$ m (sea state 4).

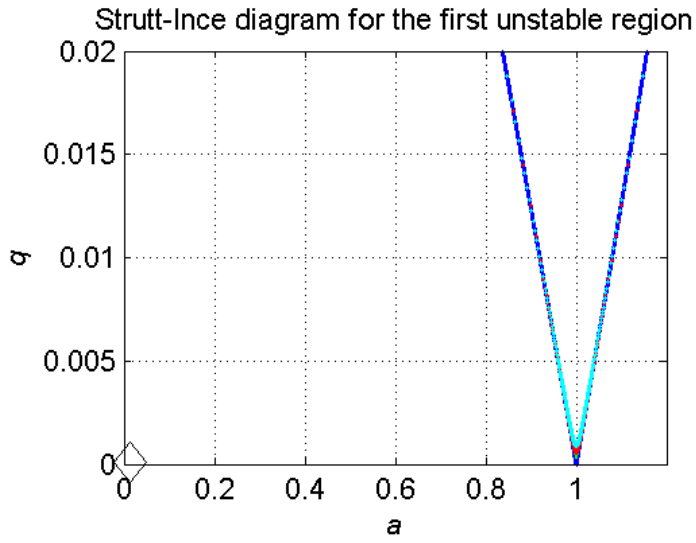

Figure 39. Strutt-Ince diagram: $T_{wave} = 8.8$ s and $A = 0.9375$ m (sea state 4).

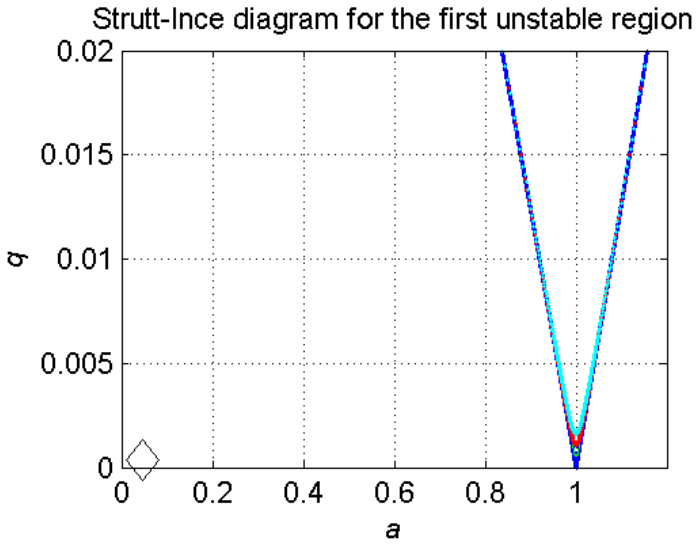

Figure 40. Strutt-Ince diagram: $T_{wave} = 16.2$ s and $A = 0.9375$ m (sea state 4).

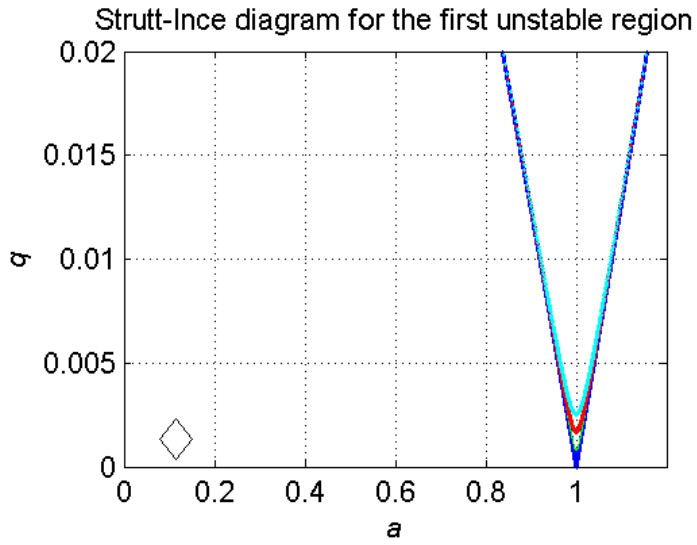

Figure 41. Strutt-Ince diagram: $T_{wave} = T_{critical}$ and $A = 1.25$ m.

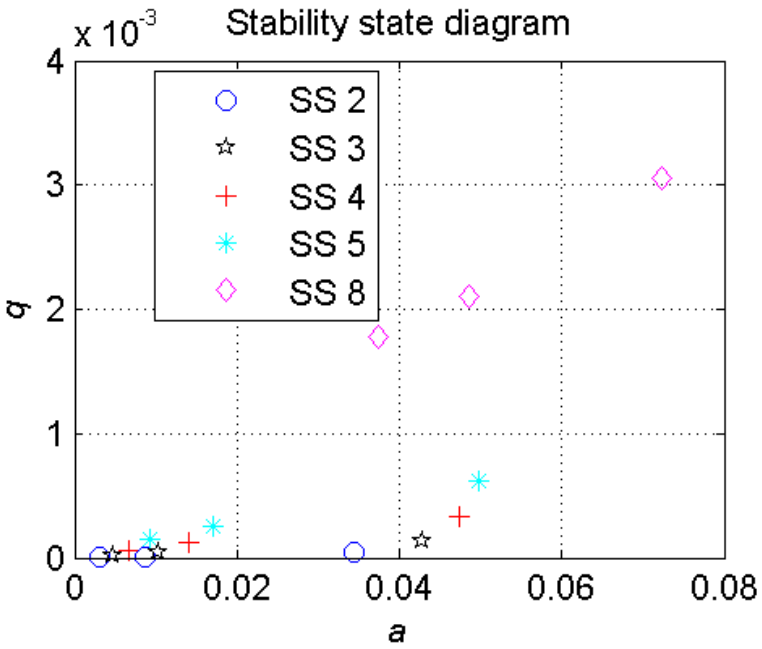

Figure 42. Combined stability state diagram for different sea states (SS).

5.6. Modified DWSC

A modified DWSC is obtained by modifying the inertial mass of the DWSC to deliberately push it into a region of unfavorable tuning. The inertial mass of this modified DWSC is found to be somewhat similar to that of a solid stepped spar of uniform density. The idea here is to show how changes in a platform's properties can lead to instances of unfavorable tuning. This small exercise helps to shine more light on the issues to keep in mind during the design process.

Some of the following results exhibit characteristics of parametric instability at a particular unfavorable tuning. Natural roll or pitch period for the modified DWSC is determined to be $\approx$ 69.0 s. The modified DWSC is forced by a regular wave of T_{wave} = 34.5 s and A = 1.25 m. The attempt here is to trigger instability by having $T_{wave} \approx \frac{1}{2} T_{n,4}$. Even though the possibility or probability of such a wave is debatable, it is nevertheless used to demonstrate parametric instability and how it is affected by viscous drag.

Figures 43 and 44 show the time histories of heave displacement and roll stiffness (determined ignoring viscous drag). A comparison of the roll stiffness variation (determined ignoring viscous drag) vs. its fit is presented in Figure 45. The corresponding Strutt-Ince diagram is presented in Figure 46. The radiated wave damping ratio for the single DOF roll EOM is determined to be 6.74e-07. The iso-damping curves on the Strutt-Ince diagram correspond to ζ = 1%, 2% and 3% respectively. Figures 47 and 48 show the time histories of sway and roll displacement (determined ignoring viscous drag).

Figures 49 and 50 show the time histories of heave displacement and roll stiffness (determined considering viscous drag). A comparison of the roll stiffness variation (determined considering viscous drag) vs. its fit is presented in Figure 51. Table 3 lists the input for the stability analysis of the modified DWSC. Figures 52 and 53 show the time histories of sway and roll displacement (determined considering viscous drag).

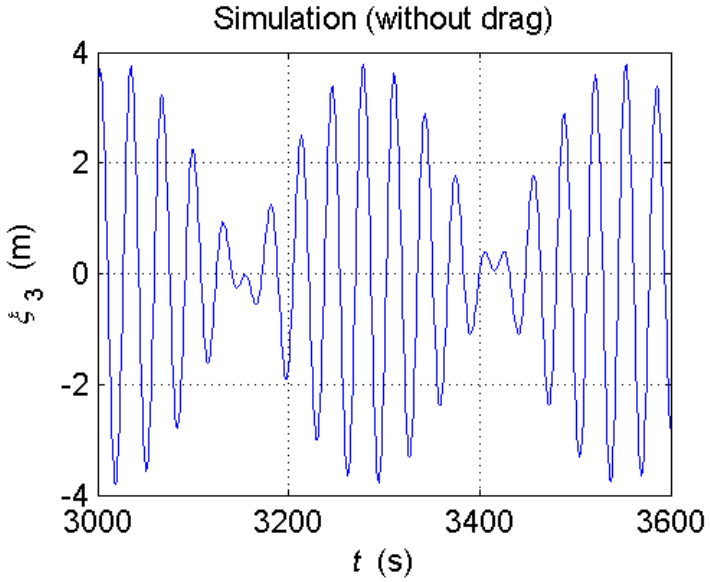

Figure 43. Heave displacement variation: $T_{wave} = 34.5$ s and $A = 1.25$ m (modified DWSC).

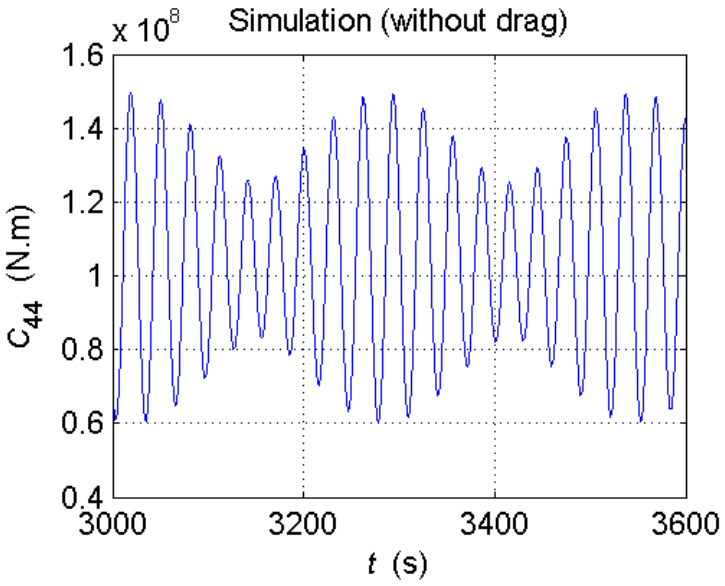

Figure 44. Roll stiffness variation: $T_{wave} = 34.5$ s and $A = 1.25$ m (modified DWSC).

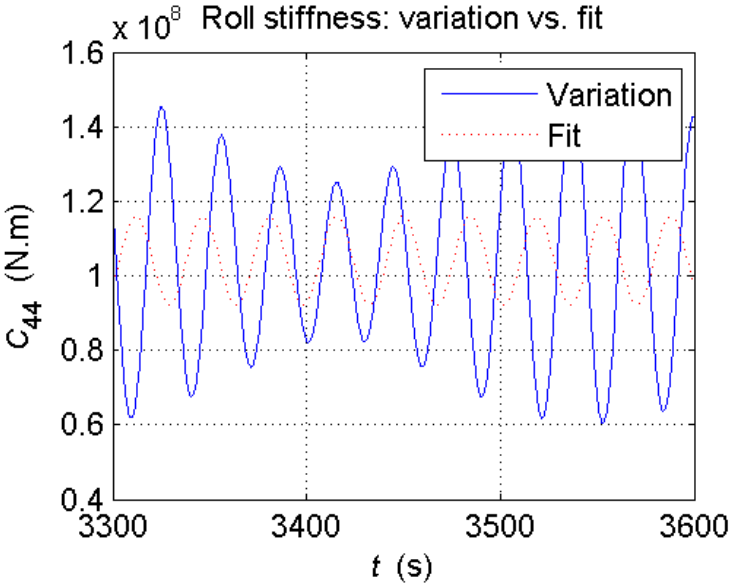

Figure 45. Roll stiffness variation vs. fit: $T_{wave} = 34.5$ s and $A = 1.25$ m (modified DWSC).

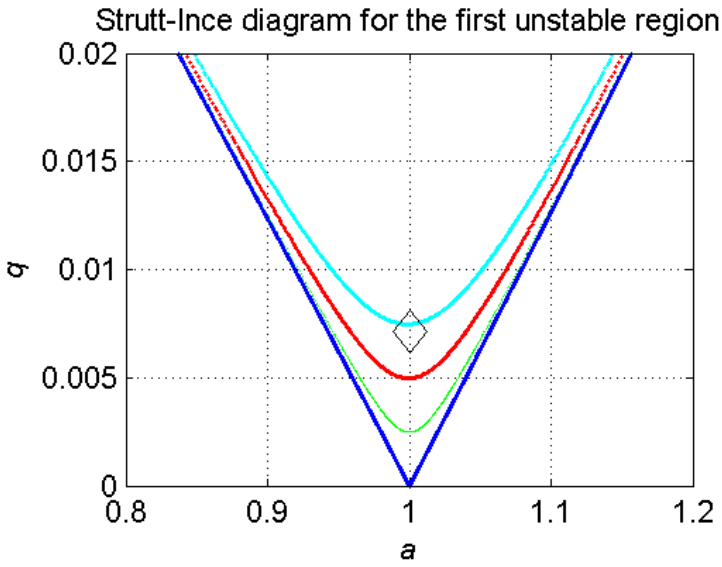

Figure 46. Strutt-Ince diagram: $T_{wave} = 34.5$ s and $A = 1.25$ m (modified DWSC).

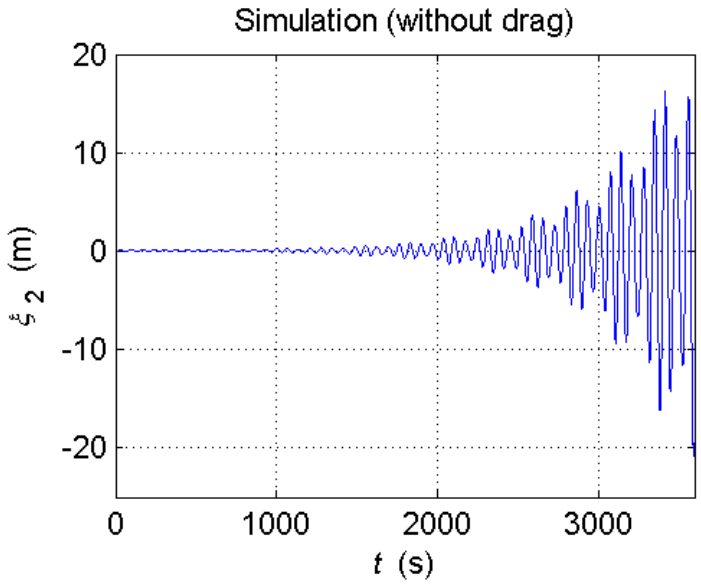

Figure 47. Sway displacement variation: $T_{wave} = 34.5$ s and $A = 1.25$ m (modified DWSC).

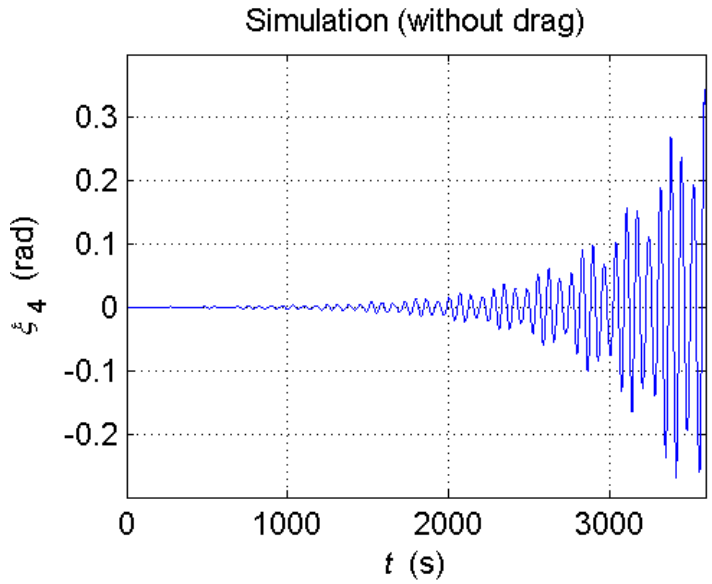

Figure 48. Roll displacement variation: $T_{wave} = 34.5$ s and $A = 1.25$ m (modified DWSC).

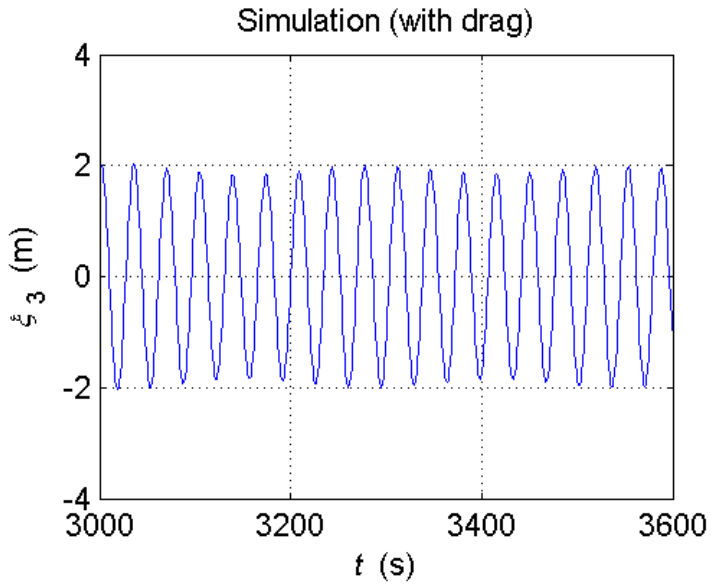

Figure 49. Heave displacement variation (drag) : $T_{wave} = 34.5$ s and $A = 1.25$ m (modified DWSC).

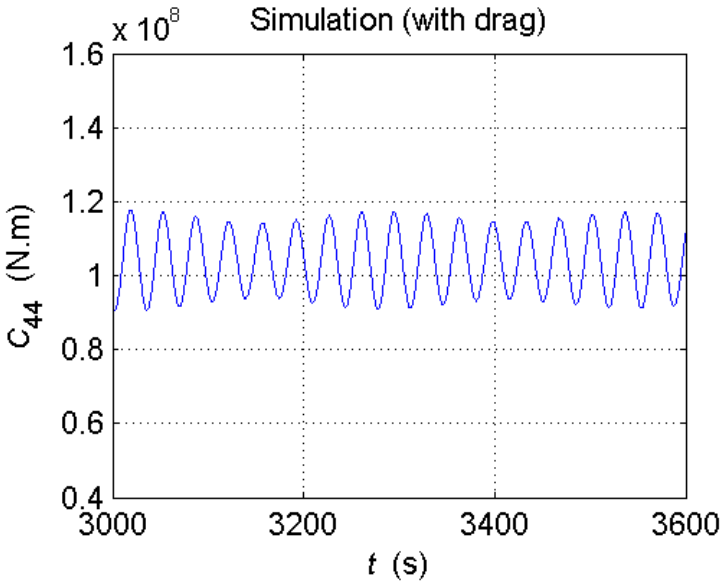

Figure 50. Roll stiffness variation (drag) : $T_{wave} = 34.5$ s and $A = 1.25$ m (modified DWSC).

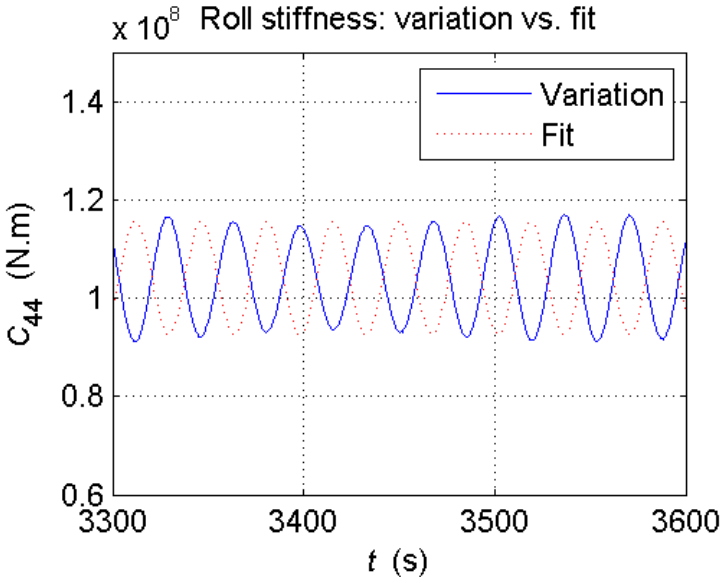

Figure 51. Roll stiffness variation vs. fit (drag) : $T_{wave} = 34.5$ s and $A = 1.25$ m (modified DWSC).

Table 3. Input data for the stability analysis of the modified DWSC.

T_{wave} (s)	A (m)	$\delta C_{44,w/o}$ (N.m)	$\delta C_{44,with}$ (N.m)	$\frac{\delta C_{44,w/o}}{C_{44,mean}}$	NATO Sea state
34.5	1.25	11880000	11500000	0.11413084	n/a

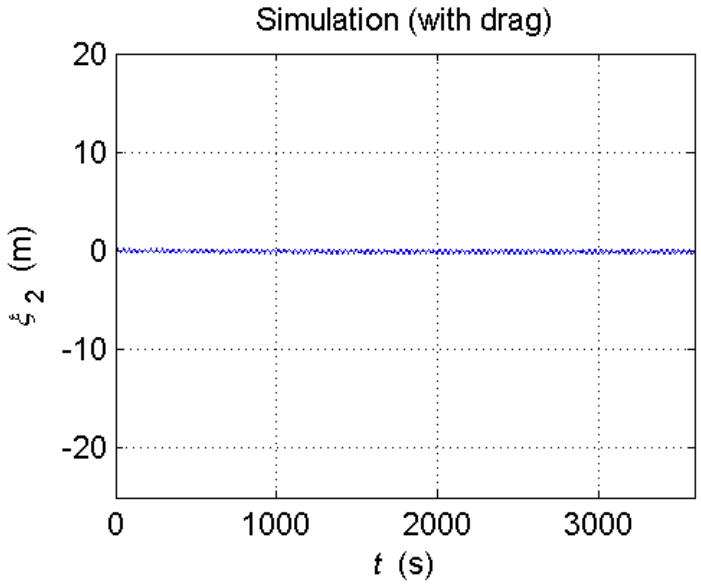

Figure 52. Sway displacement variation (drag) : $T_{wave} = 34.5$ s and $A = 1.25$ m (modified DWSC).

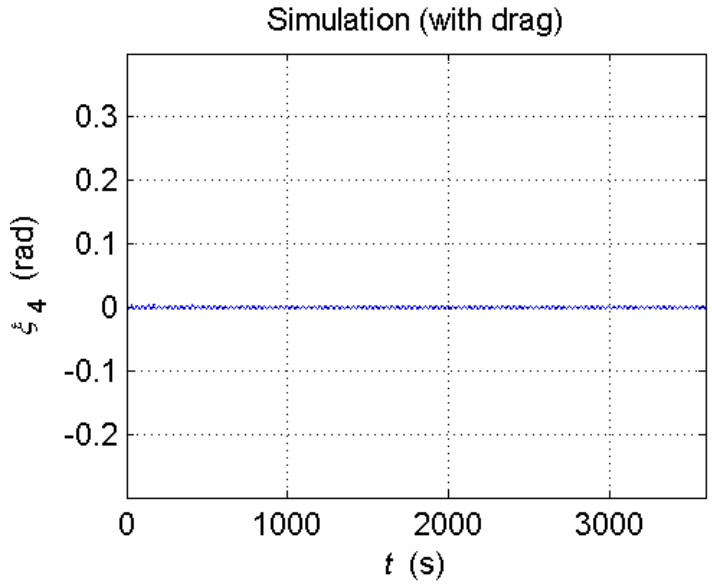

Figure 53. Roll displacement variation (drag) : $T_{wave} = 34.5$ s and $A = 1.25$ m (modified DWSC).

6. ANALYSIS OF RESULTS

6.1. Format of analysis of results

The results in this thesis are analyzed in the same order in which they are presented.

6.2. DWSC: frequency-domain

In section 5.2 plots of heave wave exciting force vs. wave frequency are presented to demonstrate a unique feature of the DWSC with respect to spars of constant cross section. Figure 3 shows a drastically reduced heave wave exciting force at 0.2398 rad/s (26.2018s). It seems that the heave wave exciting force at 0.2398 rad/s has been reduced by tuning the counteracting forces. The DWSC, by virtue of having two horizontal surfaces, may have the dynamic pressure force acting on the upper horizontal surface counteract (to some extent) the dynamic pressure force on the bottom of the DWSC. Due to the exponential decay of the wave effects with depth, a smaller area closer to the water surface produces the same counteracting effect as a larger area further away from the water surface. The fact that Haslum's and Faltinsen's $T_{critical} = 25.3118$s is close to this 'cancellation frequency' might explain why roll/ pitch resonance is not triggered.

Figure 5 contains pitch RAOs for the DWSC ($T_{n,5} \simeq 148.8$s) and the modified DWSC ($T_{n,5} \simeq 69.0$s).

6.3. DWSC: time-domain simulations

Time-domain simulations of C_{44} without and with viscous drag are presented in ascending order of sea state and then wave period. For each sea state, wave periods corresponding to 5 percentile, 95 percentile and peak frequency are considered. $C_{44,mean}$ is calculated as 104091058.8 N.m. For lower sea states, wave periods and amplitudes, viscous heave drag seems to have very little effect.

$C_{44}(t)$, ξ_3, ξ_2 and ξ_4 are then investigated for $T_{wave} = T_{critical}$ and $A = 1.25$m. ξ_2 and ξ_4 simulations are meant to validate the prediction of stability or instability of the DWSC (predicted using the Strutt-Ince diagram). Viscous drag is seen to have a significant influence on ξ_3, ξ_2 and ξ_4 but not so much on $C_{44}(t)$.

6.4. DWSC: Fourier analysis

Fourier analysis of both $C_{44}(t)$ shows very little difference between $\delta C_{44,w/o}$ and $\delta C_{44,with}$. Therefore $\frac{\delta C_{44,w/o}}{C_{44,mean}}$ is used in the stability analysis. The difference might not be negligible for higher harmonics.

6.5. DWSC: stability analysis

For T_{wave} s and A s considered corresponding to sea states 2 to 4 the point denoting the stability/ instability state falls far away from the instability region. $T_{wave} = T_{critical}$ and $A = 1.25$m has similar result. A diagram combining the presented stability states (Figures 32-40) and those corresponding to sea states (SS) five and eight is shown in Figure 42 to highlight that with higher sea states, wave periods and

amplitudes the points denoting the stability or instability state move relatively closer to the instability region.

6.6. Modified DWSC

The modified DWSC is a deliberate attempt to showcase parametric instability. It also helps in validating the methodology used in this thesis to predict/ detect parametric instability.

Fourier analysis of $C_{44}(t)$ shows very little difference between $\delta C_{44,w/o}$ and $\delta C_{44,with}$. Therefore it really does not matter whether one uses $\delta C_{44,w/o}$ or $\delta C_{44,with}$ in the stability analysis. Considering $C_{44}(t)$ without viscous drag, a Strutt-Ince diagram with the point, denoting the stability/ instability state, falling just below the 3% damping ratio curve results. As the radiated wave damping ratio for the unforced roll EOM is 6.74e-07, therefore the modified DWSC is susceptible to parametric instability. This is corroborated by ξ_2 and ξ_4 simulations without viscous drag.

If viscous heave drag is considered and viscous sway and roll drag are not considered, then the Strutt-Ince diagram changes very little as there is very little difference between $\delta C_{44,w/o}$ and $\delta C_{44,with}$. This implies that viscous heave drag is not really affecting parametric instability at this particular combination of T_{wave} and A. This fact is validated by ξ_2 and ξ_4 simulations with viscous drag. Viscous sway and roll drag are seen to stop the parametric instability from occurring. This implies that viscous roll drag probably pushes the damping ratio for the unforced roll EOM to 3% or above it.

Figure 45 is presented to highlight an instance where modeling the roll stiffness variation as a sum of a mean with one harmonic is not an accurate description of the roll stiffness variation. Figure 51 shows how the consideration of viscous drag allows a better description of the roll stiffness variation as a sum of a mean with one harmonic in comparison to when viscous drag is ignored. Therefore when the roll stiffness variation cannot be adequately described by a mean and one harmonic and when points, denoting stability states, are close to an instability region, a Hill's equation based stability analysis might be required.

7. CONCLUSIONS

The following conclusions are reached in this thesis:

1) Parametric instability is not found for the DWSC. The reason why parametric instability is not triggered is because:
   a) the natural period in heave is nowhere close to half the natural period in roll
   b) there is not considerable wave energy at half the natural period in roll
2) Roll resonance is not triggered when $T_{wave} = T_{critical}$ as $T_{critical} =$ 25.3118s is close to a 'cancellation point' vis-à-vis heave wave exciting force.
3) The DWSC has to be modified considerably to make it susceptible to parametric instability.
4) Viscous drag does not seem to have significant effect at lower sea states, wave periods and amplitudes.
5) The difference between $\delta C_{44,w/o}$ and $\delta C_{44,with}$ might be negligible but the same might not be true for higher harmonics. This could be important for a stability analysis based on Hill's equation.
6) With higher sea states, wave periods and amplitudes the points denoting the stability state move relatively closer to the instability region.
7) Viscous sway and roll drag are seen to strongly effect the possibility of parametric instability.
8) The DWSC seems to avoid heave resonance by:

a) having increased damping: the DWSC because of its stepped nature has an additional horizontal surface for viscous drag to act.

b) pushing the natural period out of the wave energy range: DWSC's non-constant cross section increases the added mass. Also its decreased waterplane area increases its natural period.

c) reducing the heave exciting force: the DWSC because of its stepped nature reduces the heave exciting force by tuning counteracting forces.

9) Further investigation of the DWSC with respect to second-order effects (especially difference frequency) might be needed as natural periods of the DWSC are relatively high.

10) When the roll stiffness variation cannot be adequately described by a mean and the first harmonic and when points, denoting stability states, are close to an instability region, a Hill's equation based stability analysis might be required.

11) Stability analysis should be extended to 'realistic' seaways.

REFERENCES

Chakrabarti, S.K., 2005. Handbook of offshore engineering. Elsevier, London.

Das, S., 2000. Transit draft roll motion stability analysis of the mobile offshore base using time varying coefficients. M.S. thesis, University of New Orleans, 2000.

Das, S., Falzarano, J., 2001. Transit draft roll motion stability analysis of the mobile offshore base (MOB) using time varying coefficients. In: Proceedings of the 11th International Offshore and Polar Engineering Conference, 2001, Stavanger, Norway.

Dern, J-C., 1972. Unstable motion of free spar buoys in waves. In: Proceedings of the 9th Symposium of Naval Hydrodynamics, 1972, Paris.

Falzarano, J.M., Cheng, J., Das, S., 2003. Parametric excitation of floating offshore platforms. In: Proceedings of the 8th International Conference on the Stability of Ships and Ocean Vehicles, 2003, Escuela Técnica Superior de Ingenieros Navales.

Francescutto, A., 2001. An experimental investigation of parametric rolling in head waves. Journal of Offshore Mechanics and Arctic Engineering, 123, 65-69.

Haslum, H.A., Faltinsen, O.M., 1999. Alternative shape of spar platforms for use in hostile areas. In: Proceedings of 1999 Offshore Technology Conference, May 3-6, 1999, Houston, Texas, OTC 10953.

Hayashi, C., 1964. Nonlinear oscillations in physical systems. McGraw-Hill, New York.

Koo, B.J., Kim, M.H., Randall, R.E., 2004. Mathieu instability of a spar platform with mooring and risers. Ocean Engineering, 31, 2175-2208.

Liao, S.-W., Yeung, R.W., 2001. Investigation of the Mathieu instability of roll motion by a time-domain viscous-fluid method. In: Proceedings of the 16th International Workshop on Water Waves and Floating Bodies, April, 2001, Hiroshima, Japan.

Rho, J.B., Choi, H.S., Lee, W.C., Shin, H.S., Park, I.K., 2002. Heave and pitch motions of a spar platform with damping plate. In: Proceedings of the 12th International Offshore and Polar Engineering Conference, 2002, Kitakyshu, Japan.

Selfridge, M., 2005. Spar technology as a seabasing enabler. Center for Innovation in Ship Design/ Naval Surface Warfare Center Carderock Division, West Bethesda, Maryland, USA.

Tao, L., Lim, K.Y., Thiagarajan, K., 2004. Heave response of classic spar with variable geometry. Journal of Offshore Mechanics and Arctic Engineering, 126, 90–95.

Zhang, L., Zou, J., Huang, E.W., 2002. Mathieu instability evaluation for DDCV/ SPAR and TLP tendon design. In: Proceedings of the 11th Offshore Symposium, The Society of Naval Architects and Marine Engineers (SNAME), 2002, Houston, Texas.

VITA

Name:	Chandan Lakhotia
Address:	Coastal & Ocean Engineering Division Zachry Department of Civil Engineering Texas A&M University, 3136 TAMU, College Station, TX 77843
Email Address:	chandan.lakhotia@gmail.com
Education:	B.Tech., Civil Engineering, National Institute of Technology, Calicut, 2007 M.S., Ocean Engineering, Texas A&M University, 2010